AD-A067 789 HUGHES RESEARCH LABS MALIBU CALIF F/G 20/6
BLUE-GREEN FILTER TECHNOLOGY.(U)
MAR 79 J F LOTSPEICH, D M HENDERSON N00014-78-C-0201
UNCLASSIFIED NL

1 OF 1
AD
A067789

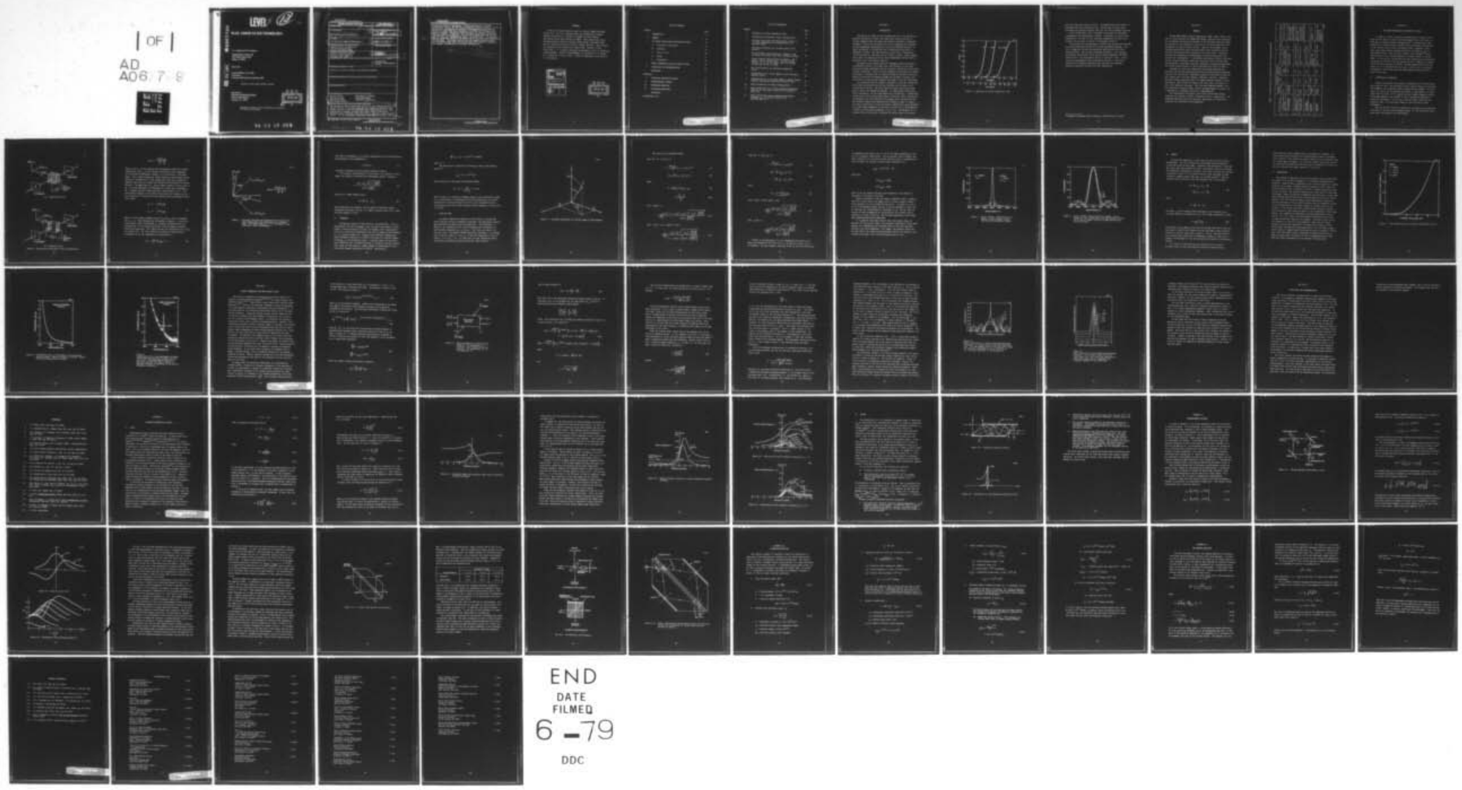

END
DATE
FILMED
6-79
DDC

BLUE–GREEN FILTER TECHNOLOGY

J.F. Lotspeich and D.M. Henderson

Hughes Research Laboratories
3011 Malibu Canyon Road
Malibu, CA 90265

March 1979

Contract N00014–78–C–0201
Final Report
1 February 1978 through 31 December 1978

Approved for public release; distribution unlimited.

Sponsored by
PHYSICAL SCIENCES DIVISION
Office of Naval Research
Arlington, VA 22217

DDC
RECEIVED
APR 18 1979
RECEIVED
D

UNCLASSIFIED

SECURITY CLASSIFICATION OF THIS PAGE (When Data Entered)

REPORT DOCUMENTATION PAGE

READ INSTRUCTIONS BEFORE COMPLETING FORM

1. REPORT NUMBER
2. GOVT ACCESSION NO.
3. RECIPIENT'S CATALOG NUMBER

4. TITLE (and Subtitle)

⑥ BLUE-GREEN FILTER TECHNOLOGY.

5. TYPE OF REPORT & PERIOD COVERED

⑨ Final Report.

1 Feb [redacted] - 31 Dec [redacted]78

6. PERFORMING ORG. REPORT NUMBER

7. AUTHOR(s)

⑩ J.F. Lotspeich [redacted] D.M. Henderson

8. CONTRACT OR GRANT NUMBER(s)

⑮ N00014-78-C-0201

9. PERFORMING ORGANIZATION NAME AND ADDRESS

Hughes Research Laboratories
3011 Malibu Canyon Road
Malibu, California 90265

10. PROGRAM ELEMENT, PROJECT, TASK AREA & WORK UNIT NUMBERS

11. CONTROLLING OFFICE NAME AND ADDRESS

Physical Sciences Division
Office of Naval Research
Arlington, VA 22217

12. REPORT DATE

⑪ Mar[redacted]79

13. NUMBER OF PAGES

⑫ 73p.

14. MONITORING AGENCY NAME & ADDRESS (if different from Controlling Office)

15. SECURITY CLASS. (of this report)

UNCLASSIFIED

15a. DECLASSIFICATION DOWNGRADING SCHEDULE

16. DISTRIBUTION STATEMENT (of this Report)

Approved for public release; distribution unlimited.

17. DISTRIBUTION STATEMENT (of the abstract entered in Block 20, if different from Report)

18. SUPPLEMENTARY NOTES

19. KEY WORDS (Continue on reverse side if necessary and identify by block number)

Optical filter
Blue-green band
Narrow pass band
Wide field of view
Electrooptic coupling
Four-wave mixing
Dispersive reflection

20. ABSTRACT (Continue on reverse side if necessary and identify by block number)

approx.

New concepts in wide field-of-view ($\sim$ f/0.5), very narrow band ($\sim$0.1 Å) optical filters in the blue-green spectral region are sought for submarine receivers in the Navy OPSATCOM laser communication link. This program was an attempt to extend the current state of the art by exploring novel techniques that would lead to improved, useful receiver filters. Of the six general approaches investigated, two were → next page

DD FORM 1 JAN 73 1473 EDITION OF 1 NOV 65 IS OBSOLETE

UNCLASSIFIED

SECURITY CLASSIFICATION OF THIS PAGE (When Data Entered)

JOB

172 600

79 04 16 024

considered principal candidates: (1) the electrooptic iso-index coupled-wave filter, and (2) nearly degenerate four-wave mixing. It was shown that a coupled-wave electrooptic filter exhibits a theoretical 2π field of view (FOV) and a passband of 0.2 Å at 4970 Å using a 1-cm sample of $AgGaS_2$. Tunability above and below the resonant wavelength was also shown to be feasible. The four-wave mixing approach also has a 2π FOV and, with adequate pump power, can exhibit gain. Very narrow optical bandwidths (~0.08 Å) and maximum skirt rejection were demonstrated theoretically. The latter approach has the biggest potential payoff but the highest risk, while the coupled-wave EO technique is basically very simple, limited only by materials availability.

2pi

approx

FOREWORD

This is the final technical report on Contract N00014-78C-0201, Project 421. The work reported herein was accomplished by Hughes Research Laboratories, a division of Hughes Aircraft Company, 3011 Malibu Canyon Road, Malibu, CA 90265. This research was accomplished during the period 1 February 1978 through 31 December 1978. The U.S. Navy program monitor was M. B. White, Code 421. This document was submitted by the authors on 28 March 1979. Authors of this report were J. F. Lotspeich, principal investigator, and D. M. Henderson, program manager. Special acknowledgement is extended to D. M. Pepper, R. L. Abrams, M. B. Klein, and D. T. Hon for significant contributions to this program.

TABLE OF CONTENTS

SECTION PAGE

1 INTRODUCTION 9
2 SUMMARY 13
3 ISO-INDEX COUPLED-WAVE ELECTROOPTIC FILTER 15
  A. Principles of Operation 15
  B. Linewidth 19
  C. Field of View 20
  D. Tuning 27
  E. Transmission 28
4 NEARLY DEGENERATE FOUR-WAVE MIXING FILTER 33
5 CONCLUSIONS AND RECOMMENDATIONS 43
REFERENCES 45

APPENDICES

I DISPERSIVE REFLECTION FILTERS 47
II INTERFEROMETER APPROACH 57
III HETERODYNE DETECTION 67
IV THE QUANTUM AMPLIFIER 71
REFERENCES 75
DISTRIBUTION LIST 77

[redacted]

LIST OF ILLUSTRATION

FIGURE		PAGE
1	Dependence of filter bandwidth on FOV	10
2	Coupled-wave electrooptic filter configurations . . .	16
3	Principal directions and characteristic values of the index eigenvectors with application of an external field	18
4	Coordinate definition for off-axis waves in FOV analysis	21
5	Filter transfer characteristics of $AgGaS_2$, 10 mm in length, for on-axis rays with half-wave voltage .	25
6	Filter transfer characteristics of $AgGaS_2$, 1 mm in length: (I) for on-axis rays, (II) for extreme off-axis ray in the X-Y plane, (III) for extreme off-axis ray in the Y-Z plane	26
7	FOV characteristics for modified coupled-wave filter	29
8	Transmission loss in (110) $AgGaS_2$ in the blue-green spectral region	30
9	Transmission loss in the same sample of $AgGaS_2$ between parallel polarizers aligned with the optic axis . . .	31
10	Nearly degenerate four-wave mixing geometry	35
11	Power reflectivity, R, versus normalized wavelength detuning Ψ, for several values of the nonlinear gain, $\lvert\kappa\rvert L$	40
12	Power reflectivity versus normalized wavelength detuning, Ψ, for several values of the nonlinear gain, $\lvert\kappa\rvert L$	41

SECTION 1

INTRODUCTION

The ability of light in the blue-green portion of the spectrum to penetrate sea water to operational depths has created interest in optical communications from space and airborne platforms to submerged terminals. Of the various blue/green optical communications programs, the most demanding requirements are set by the OPSATCOM scenario, in which information is transmitted from a synchronous satellite to a submarine at depth. The link requires a filter with a bandwidth of $\sim$0.1 Å and field of view (FOV) of $\pm 45^{\circ}$ ($\sim$f/0.5 optics). These requirements cannot be simultaneously met with conventional filters (such as dielectric layer interference filters).

Although optical communications to submerged stations has been of considerable interest to the Navy since the invention of the laser, projected systems performance has been severely limited by the available receiver technology. Several factors complicate the problem in a marine environment, including loss of coherence caused by multiple scattering, wavefront distortion in passing through the air-water interface, and uncertainty in pointing that requires the target to be over illuminated.

The blue-green filters require a wide FOV to allow the transmitted laser light scattered by the air-sea interface and sea water to be efficiently collected. The filter must also have a very narrow pass band to reject the background sunlight. In conventional interference filter approaches, the two requirements are contradictory. Conventional interference filters include Fabry-Perot, dielectric layer interference, acoustooptic, and electrooptical birefringent (Lyot and Solc) filters. The tradeoff between pass bandwidth and f/number is shown in Figure 1 for three acoustooptic filters operating at 5000 Å with a pass bandwidth of $\Delta\lambda_0$ for large f/numbers. We see that a filter with a 1-Å passband at f/50 has its performance degraded to 2 Å at $\sim$f/7. Furthermore, it is evident from the curve that a 1-Å-wide f/1 filter cannot be achieved

[redacted]

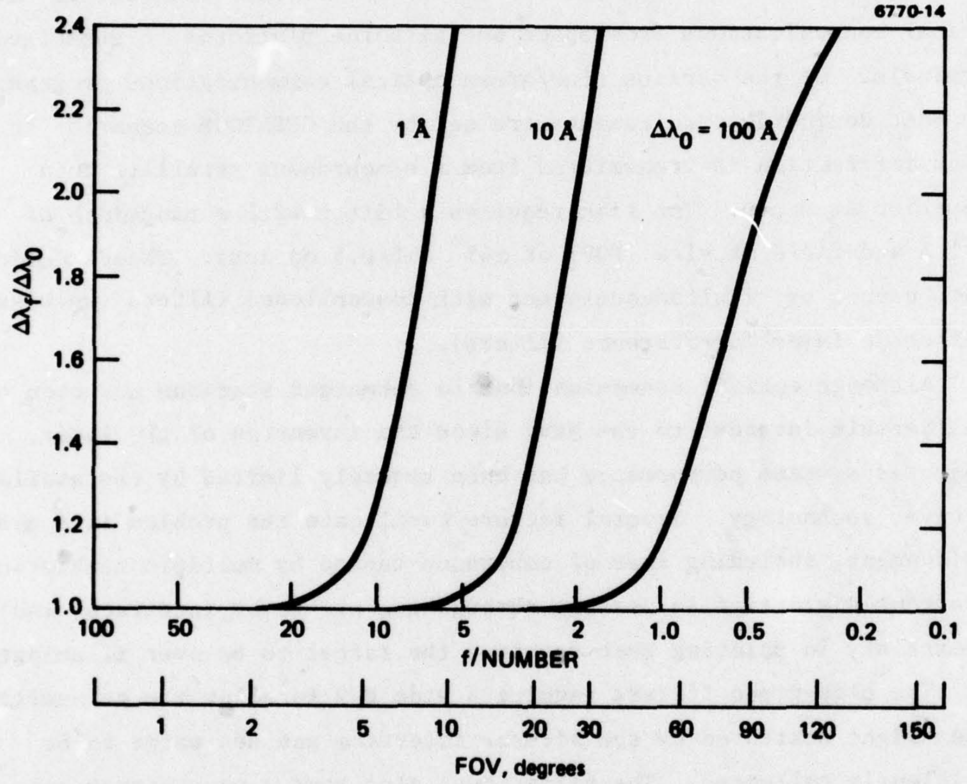

Figure 1. Dependence of filter bandwidth on FOV.

with this type (and class) of filter. Although filters that operate on wavelength-selective scattering (e.g., Christiansen filters) could eliminate this tradeoff problem, they lack the narrow passband required.

Since conventional filter techniques cannot meet the blue-green requirements, new approaches are needed. A modified Lyot filter with a linewidth of ∿1 Å, FOV of ±30°, and peak transmission of ∿40% is projected to be the state of the art in blue/green filters.*

The purpose of our program was to explore new concepts for wide FOV, very narrow linewidth filters for the Navy blue/green programs. Section 2 summarizes the various approaches explored and lists their characteristics. The two most promising techniques — the iso-index coupled-wave electrooptic filter and the nearly degenerate four-wave mixing filter — are discussed in detail in Sections 3 and 4. Conclusions and recommendations are presented in Section 5. The report concludes with separate appendices that describe the remaining approaches explored and point out their limitations.

---

*Lockheed is presently under contract to fabricate such a filter.

SECTION 2

SUMMARY

During 1978, Hughes Research Laboratories (HRL), under contract with the U.S. Navy (Contract No. N00014-78-C-0201), explored novel techniques for narrowband filtering with wide FOV in the blue-green spectral region. The purpose of this exploratory study was to lay the groundwork for the development of useful receiver filters. Early in the program, brainstorming sessions were held involving senior staff scientists and consultants having specialized competence in related fields. From these sessions and independent interim studies, six general approaches were selected for investigation: coupled-wave electrooptic filters, four-wave optical mixing techniques, dispersive reflective filters, white-light interferometers, heterodyne detection techniques, and quantum amplifiers. The salient characteristics of these approaches are listed in Table 1.

Although the first three approaches each showed potential for providing the wide FOV characteristics and the narrow optical bandwidths required, the electrooptic coupled-wave approach is believed to show the most promise with the least expense, complexity, and risk. Although four-wave mixing techniques offer the biggest potential payoff in filter performance, they present the highest risk since they are based on a new, still immature technology. The third best approach appears to be the dispersive reflective filter, which, although simple in concept, has a high degree of complexity and risk in implementation.

The coupled-wave electrooptic filter and the four-wave mixing technique are analyzed in detail in Sections 3 and 4, respectively. The remaining approaches and their principal limitations (or reasons for exclusion) are discussed in the appendices.

Table 1. Characteristics of Blue-Green Filter Techniques Explored

Operating Principle	Estimated Linewidth	Estimated Interaction FOV	Estimated Interaction Efficiency	Fixed or Tunable	Complexity	Additional Comments
1. Coupled-wave electro-optic filter	0.2 Å	2π	$\sim$40% 50% max	Tunable by temperature or composition	Low	Calculated for $AgGaS_2$
2. Nearly degenerate four-wave mixing	0.08 Å for 1 cm length	2π	$\sim$100%	Tunable by pump laser selection	High	Gain can be realized with this approach (i.e., reflection efficiencies >100%)
3a. Dispersive reflector (cesium vapor)	0.5 Å	$\sim$f/0.5	$\sim$20%	Fixed by absorption line	Medium	Requires handling of metal vapors
3b. Dispersive reflector (rare earth ion)	0.1 Å <77°K	$\sim$f/0.5	60%	Fixed by absorption line	Low	Can be multipassed to improve out-of-band rejection (10^{-5})
4. White-light interferometer	0.1 Å	$\sim$f/1.5	$\sim$50%	Fixed by absorption line	High	
5. Heterodyne detection	8×10^{-5} Å (10 MHz)	0.5 mrad	?	Tunable by local oscillator laser selection	Excessive	Efficiency rating uncertain
6. Narrow-band amplifier	0.015 Å (2 GHz)	40 mrad	$\sim$100%	Fixed by absorption line	Medium	Argon ion laser used in calculation. Negligible gain advantage.

6447

SECTION 3

ISO-INDEX COUPLED-WAVE ELECTROOPTIC FILTER

In 1966 C.H. Henry[1] proposed and demonstrated an optical filter based on the change of sign of the birefringence that occurs near the band edge in certain uniaxial semiconductors.[2] He showed that light energy can be coupled between ordinary and extraordinary polarizations at the isotropic point either by applied strain or magnetic field. Thus, when placed between crossed polarizers, the material acts as a narrow-band filter. More recently, Laurenti and co-workers[3,4] have demonstrated a filter tuning capability in mixed crystals of CdS and CdSe. In this section, we show how the wave coupling can be achieved by an applied dc electric field and propose the use of $AgGaS_2$ as a highly selective filter material at 4970 Å. The FOV characteristics are analyzed, and it is concluded that this type of filter can, in principle, accommodate a 2π FOV with less than 20% passband increase over the narrow field case.

A. PRINCIPLES OF OPERATION

Figure 2 illustrates two possible configurations of a coupled-wave electrooptic filter. The particular type of crystal chosen is one having $\bar{4}2m$ symmetry, for purposes of later illustration and example. As indicated, the filter can be operated with either a longitudinal or a transverse electric field. In the case of the most common hexagonal crystals having 6mm symmetry, such as CdS,[1-4] only a transverse-field mode of operation is possible. In all cases, the optic axis, denoted by the direction <001>, is in the plane normal to the direction of light propagation.

When an electric field $\mathcal{E}_1$ is applied in the direction as indicated, a rotation of the optic axis through an angle α in the transverse plane takes place, according to the relationship

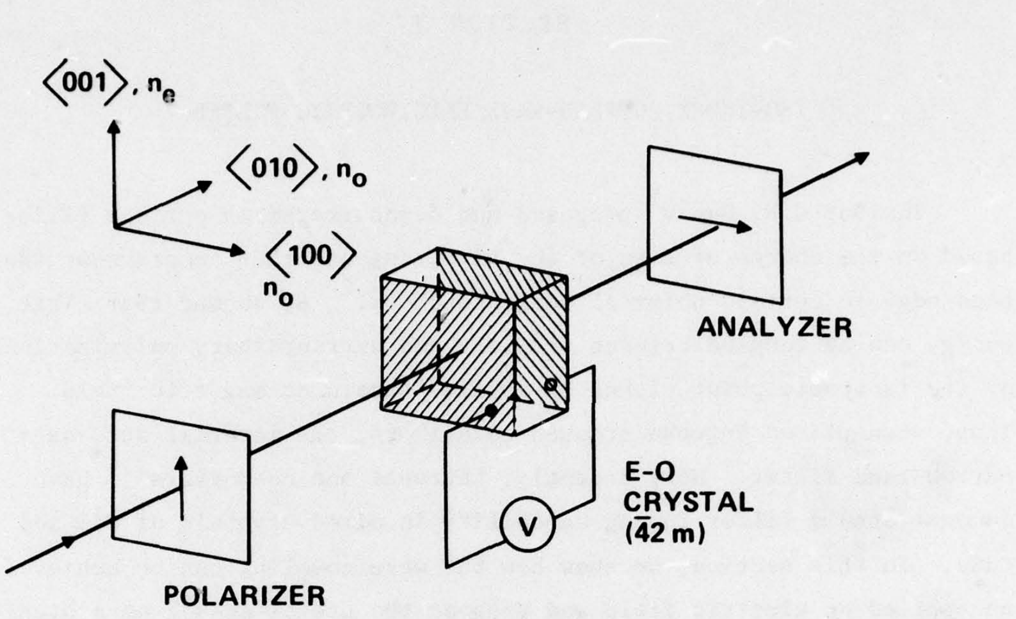

(a) Longitudinal field

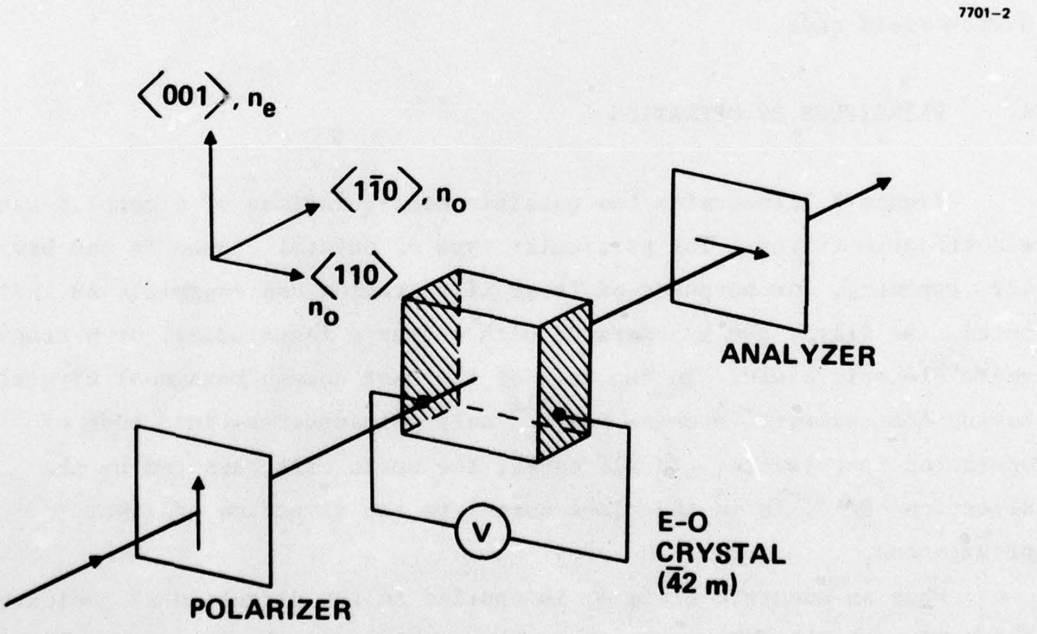

(b) Transverse field

Figure 2. Coupled-wave electrooptic filter configuration.

$$\tan 2\alpha = \frac{2n_o^2 n_e^2 r_{41}\mathscr{E}_1}{n_o^2 - n_e^2}, \tag{1}$$

where n_o and n_e are the ordinary and extraordinary refractive indexes, respectively, and r_{41} is the relevant electrooptic tensor component. For even mildly birefringent crystals, α is in practice a very small angle. Thus, light entering the crystal having its polarization either parallel or perpendicular to the orginal optic axis will essentially maintain that direction through the cyrstal and be blocked by a crossed analyzer. The magnitudes of n_o and n_e remain constant to first order in $\mathscr{E}_1$. If the birefringence now disappears at a particular wavelength λ_o, Eq. 1 becomes infinite, indicating that α goes abruptly to 45^o. The field-induced changes in the values of the refractive indexes, for the new characteristic directions of the principal axes, now depend on $\mathscr{E}_1$ in first order:

$$\begin{aligned} n_e &\rightarrow \bar{n} + \frac{1}{2}\bar{n}^3 r_{41}\mathscr{E}_1 \\ n_o &\rightarrow \bar{n} - \frac{1}{2}\bar{n}^3 r_{41}\mathscr{E}_1 \quad , \end{aligned} \tag{2}$$

where $\bar{n}$ is the average (common) value of n_e and n_o, and it is assumed that $n_e > n_o$. These features are illustrated in Figure 3. At the isotropic point, light of wavelength λ_o, linearly polarized parallel or perpendicular to the original optic axis, will now emerge in general elliptically polarized. The crystal now has the configuration of a classic Pockels cell. For that condition for which the relative phase retardation of the two eigenstates of polarization is

$$2\Gamma L = \frac{2\pi L}{\lambda_o}\bar{n}^3 r_{41}\mathscr{E}_1 = \pi \quad , \tag{3}$$

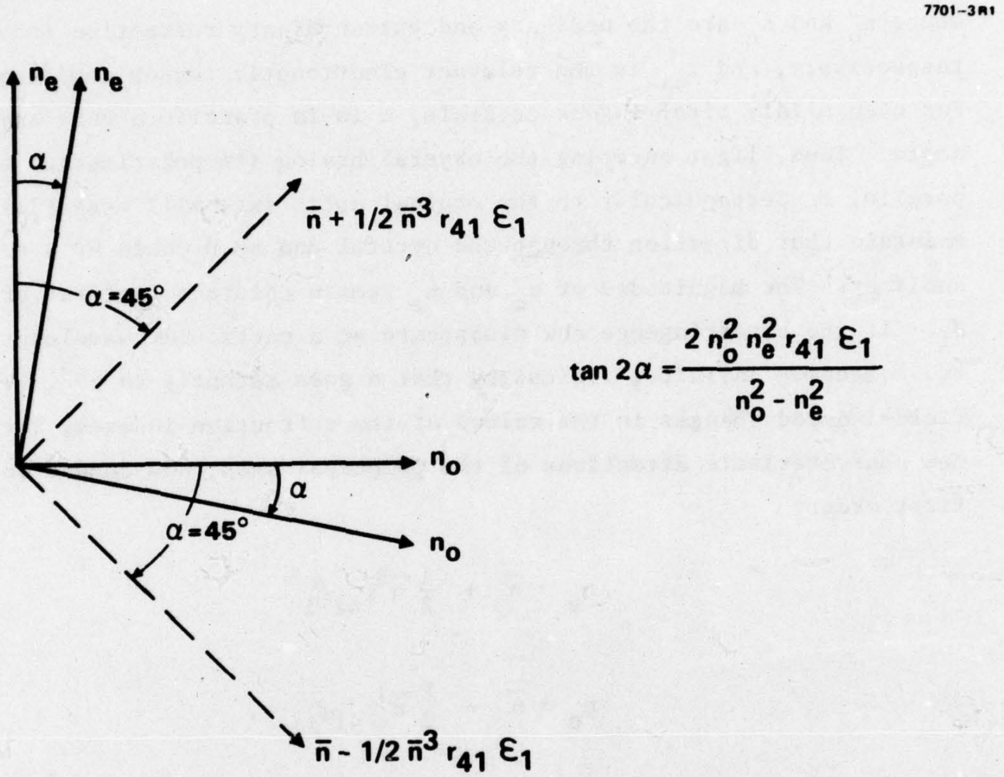

Figure 3. Principal directions and characteristic values of the index eigenvectors with application of an external field. The dashed lines at $\alpha = 45°$ correspond to the condition of zero birefringence.

the light at wavelength λ_o is totally transmitted by the crossed analyzer. More generally, the transmission is

$$\tau = \sin^2(\Gamma L) , \tag{4}$$

a familiar expression from electrooptic modulator theory.

The transfer characteristics of the filter, as a function of wavelength, can readily be derived from coupled-mode theory,[1] leading to

$$\tau = \frac{(\Gamma L)^2 \sin^2 \sqrt{(\Gamma L)^2 + \left(\frac{\Delta k L}{2}\right)^2}}{(\Gamma L)^2 + \left(\frac{\Delta k L}{2}\right)^2} , \tag{5}$$

where Δk is a phase mismatch term:

$$\Delta k = \frac{2\pi}{\lambda} (n_e - n_o) . \tag{6}$$

These expressions are familiar from the theory of nonlinear optics (parametric processes), and Eq. 4 is simply a special case of Eq. 5 when the phase mismatch is zero.

B. LINEWIDTH

An important feature of this filter is its selectivity. This is determined by the rate of change of the term $\Delta kL/2$ with respect to wavelength. Unlike acoustooptic filters, for example, this "coupled-wave" filter has a selectivity dominated by the rate at which the birefringence, $n_e - n_o$, passes through zero. Laurenti and co-workers[3] demonstrated filter passbands typically 10 to 20 Å in the green for selected samples of CdS_xSe_{1-x} a few millimeters thick. A cursory search of other materials exhibiting this accidental isotropy of refractive indices revealed that, among the chalcopyrites, $AgFaS_2$ exhibits a birefringence[5] with a very abrupt passage through zero at 4970 Å. Specifically,

$$\frac{d}{d\lambda}(n_e - n_o) = 1.87\ \mu m^{-1} \text{ at } 4970\ \text{Å},$$

and $\bar{n} = 2.7$.

The electrooptic coefficient, according to most recent measurements,[6] is

$$r_{41} = 3.2 \times 10^{-12}\ \text{m/V}.$$

These values give a half-wave field-length product

$$(\mathcal{E} \cdot L)_\pi = \frac{\lambda_o}{2\bar{n}^3 r_{41}} = 3.9\ \text{kV}.$$

Thus a crystal (or cyrstals) of $AgGaS_2$ having a total interaction length of 1 cm would have a 3-dB passband of 0.2 Å and would give full transmission with an applied voltage of 3.9 kV in the longitudinal-field configuration and 1.95 kV with transverse field, assuming a cross section of 1/4 cm^2.

C. FIELD OF VIEW

An equally important co-feature of this filter is its wide FOV. From a rigorous solution of Maxwell's equations, the generalized coupled-mode equations were derived for non-axial waves. With reference to Figure 4, we considered a wave vector $\vec{k}$ having polar coordinates θ, ϕ and Cartesian components k_x, k_z, and k_y. The Z axis was taken to be the optic axis. Two general extreme cases were considered: (1) propagation in the X-Y plane ($\phi = 0$ or $k_z = 0$) and (2) propagation in the Y-Z plane ($\phi = \pi/2$ or $k_x = 0$). For each case, we also considered results from initial polarization mostly along X and mostly along Z.

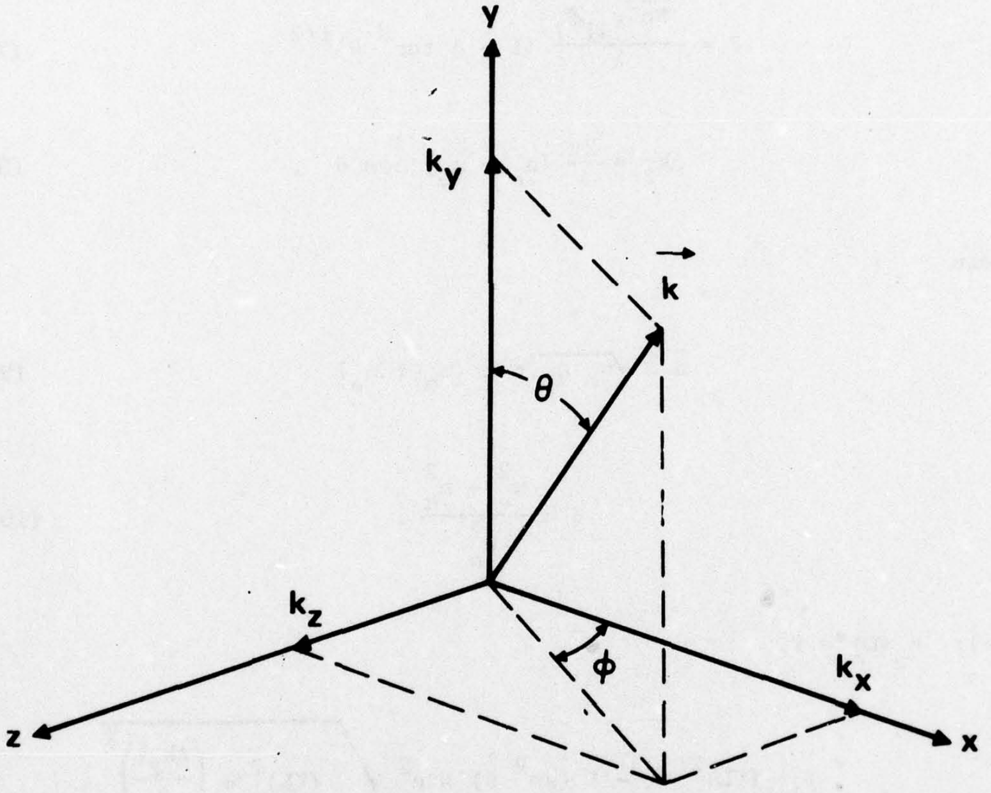

Figure 4. Coordinate definition for off-axis waves in FOV analysis.

The solutions are presented below.

Case (1): $\phi = 0$ or $k_z = 0$

$$\Gamma = \frac{\pi \bar{n}^3 r_{41} \mathscr{E}_1}{\lambda} (1 - \delta \tan^2 \theta)^{1/2} \tag{7}$$

$$\Delta k_2 = \frac{2\pi}{\lambda} (n_e - n_o) \cos \theta \quad , \tag{8}$$

where

$$\bar{n} \equiv \sqrt{n_o n_e} \cong \frac{1}{2} (n_o + n_e) \tag{9}$$

$$\delta \equiv \frac{n_e^2 - n_o^2}{n_o^2} \ . \tag{10}$$

(1a): $E_3(0) = 1.$

$$\tau = \left(\frac{\bar{n}}{n_o}\right) \frac{(\Gamma L)^2 (1 - \delta \tan^2 \theta) \sin^2 \sqrt{(\Gamma L)^2 + \left(\frac{\Delta k_2 L}{2}\right)^2}}{(\Gamma L)^2 + \left(\frac{\Delta k_2 L}{2}\right)^2} \ . \tag{11}$$

(1b): $E_1(0) = \cos \theta$, $E_2(0) = -\sin \theta$.

$$\tau = \left(\frac{\bar{n}}{n_e}\right) \frac{(\Gamma L)^2 \sin^2 \sqrt{(\Gamma L)^2 + \left(\frac{\Delta k_2 L}{2}\right)^2}}{(1 - \delta \tan^2 \theta) \left\{(\Gamma L)^2 + \left(\frac{\Delta k_2 L}{2}\right)^2\right\}} \ . \tag{12}$$

Case (2): $\phi = \frac{\pi}{2}$ or $k_x = 0$.

$$\Gamma = \frac{\pi \bar{n}^3 r_{41} \mathscr{E}_1}{\lambda} (1 + \delta \sin^2\theta)^{1/4} \tag{13}$$

$$\begin{aligned} \Delta k_2 &= \frac{2\pi}{\lambda} (n'_e - n_o) \cos\theta \\ &= \frac{2\pi}{\lambda} (n_e - n_o) \cos^3\theta \quad , \end{aligned} \tag{14}$$

where

$$n'_e = \frac{n_e}{(1 + \delta \sin^2\theta)^{1/2}} \quad . \tag{15}$$

(2a): $E_2(0) = -\sin\theta$, $E_3(0) = \cos\theta$.

$$\tau = \left(\frac{\bar{n}}{n_o}\right) \frac{(\Gamma L)^2 \sin^2 \sqrt{(\Gamma L)^2 + \left(\frac{\Delta k_2 L}{2}\right)^2}}{(\Gamma L)^2 + \left(\frac{\Delta k_2 L}{2}\right)^2} \quad . \tag{16}$$

(2b): $E_1(0) = 1$.

$$\tau = \left(\frac{\bar{n}}{n'_e}\right) \frac{(\Gamma L)^2 \sin^2 \sqrt{(\Gamma L)^2 + \left(\frac{\Delta k_2 L}{2}\right)^2}}{(\Gamma L)^2 + \left(\frac{\Delta k_2 L}{2}\right)^2} \quad . \tag{17}$$

Because of the smallness of δ, the transmission functions in all cases have essentially the form of Eq. 5, and they all reduce to Eq. 4 at resonance. We note, however, from Eqs. 8 and 14, that the selectivity is degraded by the factor cos θ or $\cos^3\theta$ for beams propagating in the x-y or y-z planes, respectively. For the specific case of $AgGaS_2$, having an index $\bar{n} = 2.7$, the most extreme off-axis angle of propagation is that for which the external incidence angle approaches π/2:

$$\theta_{max} = \sin^{-1}(1/\bar{n}) \approx 22^{\circ} .$$

This gives

$$\cos\theta_{max} = 0.929$$

$$\cos^3\theta_{max} = 0.801 .$$

Thus for the two general off-axis cases considered, the passband is increased by only about 7% and 20%.

Sample transmission curves are shown in Figures 5 and 6. Figure 5 shows the on-axis case of an $AgGaS_2$ filter, 10 mm in length, having a 3-dB passband of 0.2 Å as predicted from theory. In Figure 6, curve I is the corresponding on-axis case for a crystal thickness of only 1 mm. As expected, the 3-dB passband is increased to 2 Å. The two cases of extreme off-axis propagation are illustrated by the transfer characteristics of curves II and III. The increased passbands in both cases agree quantitatively with predictions.

It is apparent from these results that, with proper choice of material and interaction length, the iso-index coupled-wave filter shows promise of accommodating very wide FOVs while at the same time maintaining a very narrow passband. Very simply, the physical reason for the wide FOV is that optical phase matching occurs at all angles at the resonant wavelength, where the birefringence goes to zero.

7701-7

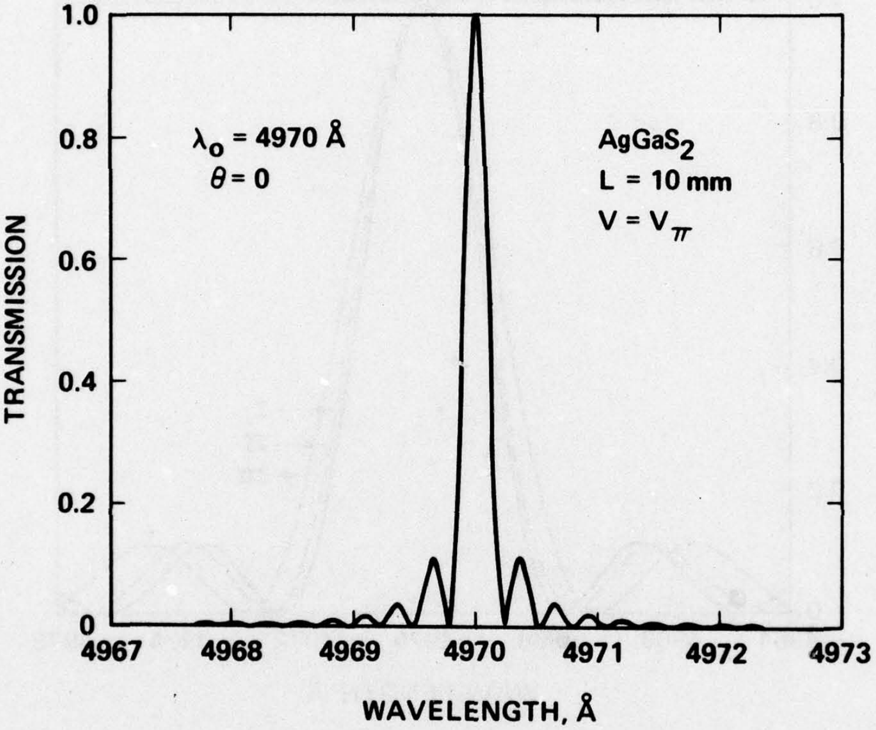

Figure 5. Filter transfer characteristics of AgGaS$_2$, 10 mm in length, for on-axis rays with half-wave voltage.

7701-10

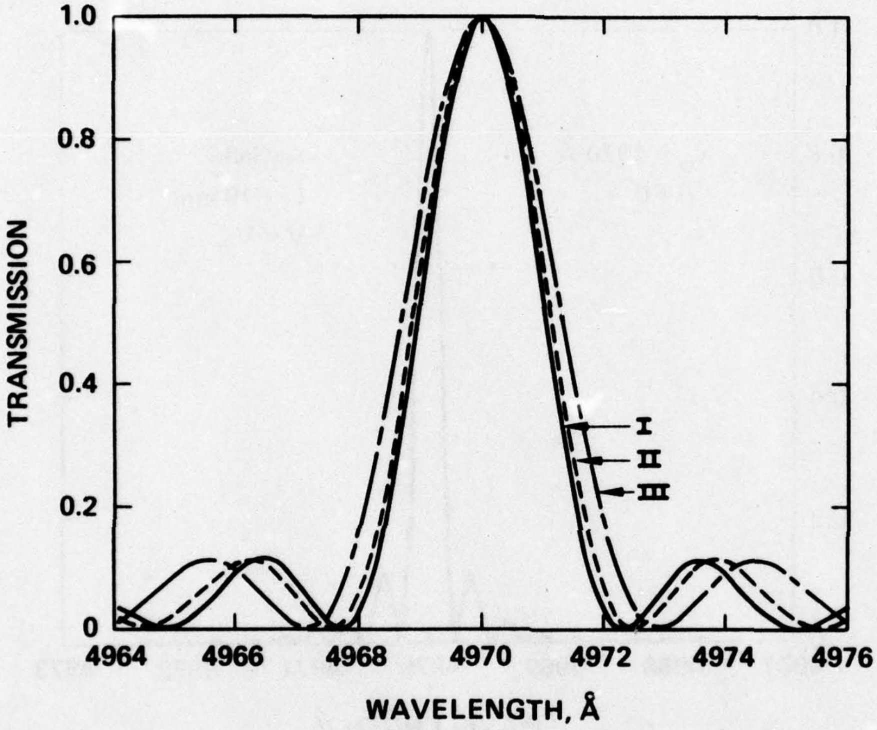

Figure 6. Filter transfer characteristics of A_gGaS_2, 1 mm in length: (I) for on-axis rays; (II) for extreme off-axis ray in the X-Y plane; (III) for extreme off-axis ray in the Y-Z plane.

D. TUNING

A nontrivial limitation of this class of optical filters needs to be mentioned. The zero crossing of birefringence characteristically occurs quite near the band edge. Therefore, some absorption of the light may result when thick samples are used. We propose a means for avoiding this problem by introducing a periodic strain field (as with the collinear acoustooptic filter[7]) or a periodic electric field following a scheme invented at Hughes several years ago for the HALO program.[8] With the periodic field of period Λ, the phase mismatch (Eq. 6) now becomes

$$\begin{aligned}\Delta k &= \frac{2\pi}{\lambda}(n_e - n_o) - \frac{2\pi}{\Lambda} \\ &= \frac{2\pi}{\lambda} C(\lambda - \lambda_o) - \frac{2\pi}{\Lambda} \quad ,\end{aligned} \tag{18}$$

where

$$C \equiv \frac{d}{d\lambda}(n_e - n_o) \tag{19}$$

and where λ_o is the original pass wavelength at the isotropic point. The phase mismatch now becomes zero at a new, longer wavelength λ_1 where

$$\Lambda = \frac{\lambda_1}{C(\lambda_1 - \lambda_o)} \quad . \tag{20}$$

We estimate that an $AgGaS_2$ filter could be retuned from 4970 Å (near the band edge) to 5100 Å (well removed from the band edge) using a periodic acoustic or electric field with a period $\Lambda \approx 32\ \mu m$. The selectivity of this retuned filter would still be dominated, however, by the rate of change of birefringence C (Eq. 19) and would thus retain its narrow band feature.

As a result of this retuning, by introduction of a directed periodic field, the FOV characteristics would be modified because phase matching would no longer occur at all angles of incidence. We have analyzed the resulting effect using existing theory for acousto-optic filters.[9] The results are shown in Figure 7 for the specific case of a 10-mm sample of $AgGaS_2$. As a specific example from these results: the half-power bandwidth for paraxial rays is increased by a factor of 3 when the external half-angle reaches 21° (f/1.3 FOV).

E. TRANSMISSION

The problem of absorptive loss at the isotropic point actually does not appear to be serious in $AgGaS_2$ if it is properly synthesized and annealed. Figure 8 shows transmission loss in the blue-green of a highly purified, clear sample of $AgGaS_2$ grown and prepared at HRL. This is a (110) platelet having a thickness of 0.84 mm. Fresnel reflective losses are not included. The residual absorptive loss near 4970 Å is less than 0.10 dB/mm. Figure 9 shows the transmission characteristics of this same sample between parallel polarizers oriented along the optic axis of the crystal. Note the 10-fold increase in spectrophotometer sensitivity. The narrow absorption line at 4970 Å results from the elastooptic polarization coupling due to a very small amount of residual strain in the crystal. It is exactly this form of polarization coupling, achieved electrooptically, that forms the basis for our coupled-wave filter using $AgGaS_2$. The linewidth is dominated by the spectrophotometer resolution of ∿3 to 5 Å. Thus, the actual material linewidth is much less. A longer interaction length of, for example, 1 cm would lead to a filter linewidth of about 0.2 Å, as estimated. Some spectral tuning caused by varying the temperature[1] is expected with $AgGaS_2$, as with CdS and CdSe, although the tuning sensitivity is not yet known. Additional tuning by compositional variations may also be feasible.[3,4] Moreover, since the sample losses illustrated in Figures 8 and 9 are so small, it might also be possible to tune to wavelengths shorter than 4970 Å by these techniques or by the periodic field approach.

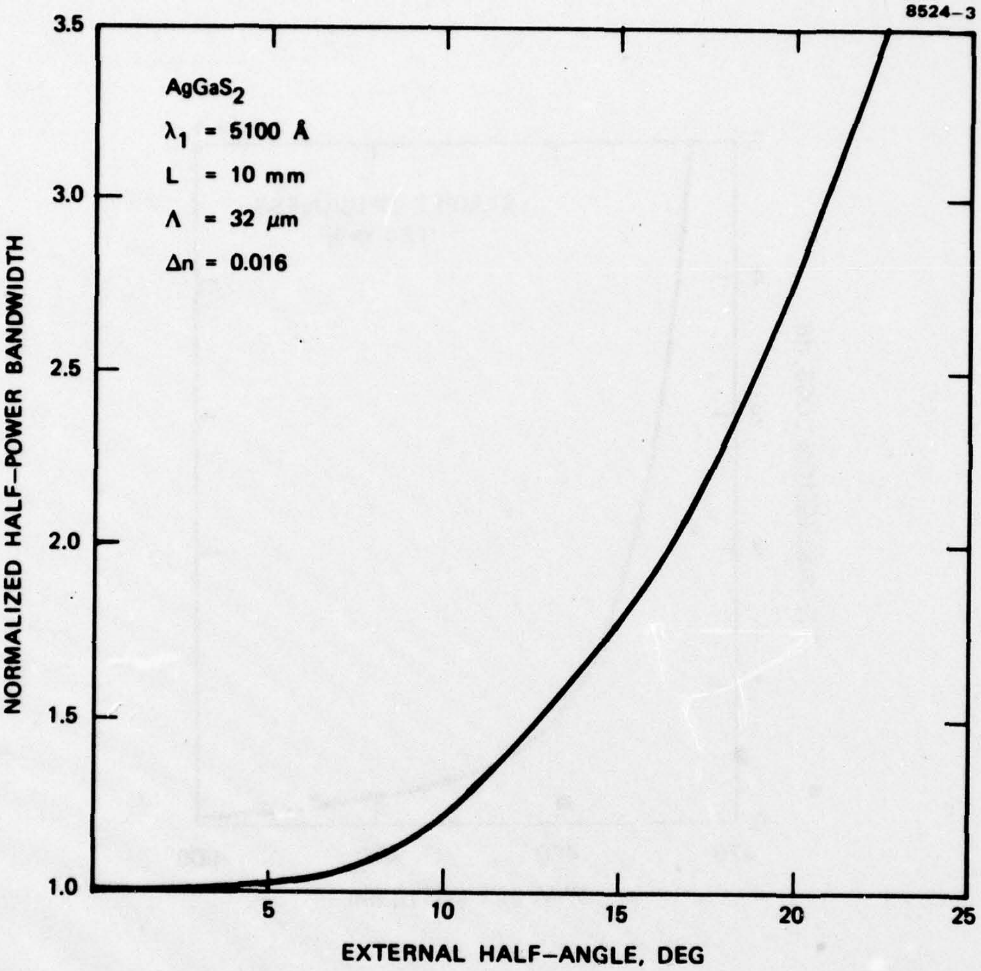

Figure 7. FOV characteristics for modified coupled-wave filter.

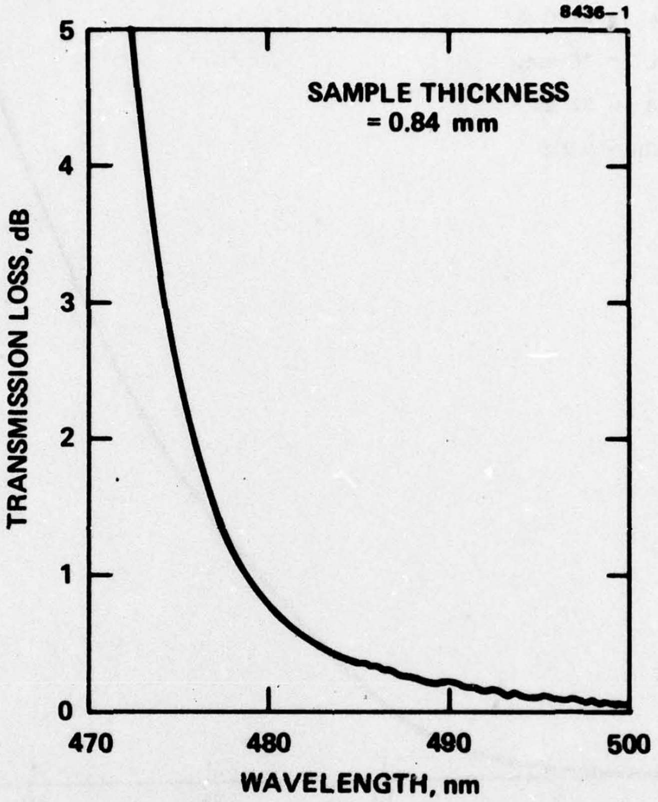

Figure 8. Transmission loss in (110) $AgGaS_2$ in the blue-green spectral region. Sample thickness is 0.84 mm. Fresnel reflection losses are not included.

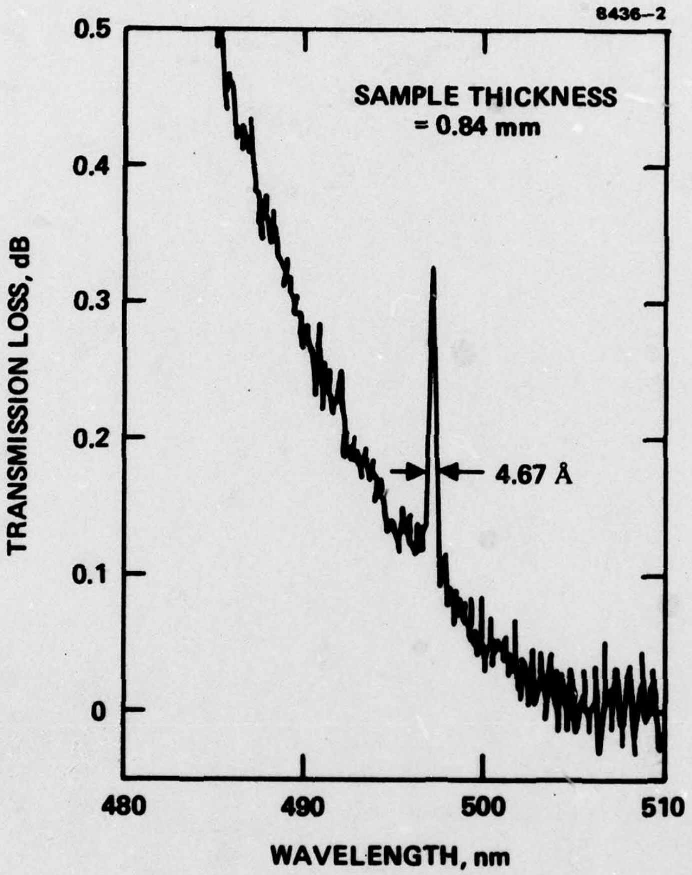

Figure 9.
Transmission loss in the same sample of $AgGaS_2$ between parallel polarizers aligned with the optic axis. Spectrophotometer sensitivity increased ten-fold over that of Figure 8. Measured linewidth is dominated by the spectrophotometer resolution.

SECTION 4

NEARLY DEGENERATE FOUR-WAVE MIXING FILTER

The process of degenerate four-wave mixing has been shown to be capable of generating phase-conjugate[10,11,12] (or "time-reversed") and amplified fields.[11,12] These effects have recently been verified experimentally.[13,14] Further, the four-wave nonlinear interaction was shown to be operationally analogous to performing real-time holography.[15] In the above efforts, all interacting fields were taken to be of the same optical frequency. During the present program, we have shown how this interaction, together with phase mismatch constraints, can be used to act as a narrow optical bandpass filter. In principle, any nonlinear interaction can be used to perform filtering functions. However, these interactions generally require a specific angle of incidence of the field to be filtered and yield an output wavelength differing from its input. Using a nearly degenerate four-wave mixing approach provides for a large FOV for the input field and an output field of essentially the same wavelength. In addition, the conjugate nature of the output field can be used to spatially filter out various "noise" fields, thus increasing the S/N performance of the filter. However, the degree of spatial filtering and detection geometry will limit the filter's FOV. Being essentially an active device, the filter will be capable of yielding an amplified output bandpass. As the filter gain increases, its bandpass will be shown to become sharper, with a concomitant decrease in the passband sidelobe structure. Finally, physical analogs with real-time holographic diffraction gratings will be shown to be consistent with the resolving power of the filter.

We assume that the interaction takes place in a nondispersive, lossless medium. Consider the frequency dependence of the amplitude of a field, E_3, generated as a result of a nonlinear interaction involving the simultaneous incidence of two intense counter-propagating "pump" fields, E_1 and E_2, of frequency ω, on a medium possessing a third-order nonlinear optical susceptibility, $\chi_{NL}^{(3)}$. Also incident (simultaneously) on the medium is a third weak field, E_4, of frequency $\omega + \delta (\delta/\omega << 1)$, propagating along an arbitrary direction. The geometry is shown in Figure 10. The fields are taken as

$$E_i(r_i) = \frac{1}{2} A_i(r_i) e^{i(\omega_i t - \vec{k}_i \cdot \vec{r}_i)} + \text{c.c.} \ , \tag{21}$$

where r_i is the distance along $\vec{k}_i$. Without loss of generality, we assume that $\chi_{NL}^{(3)}$ is polarization and frequency invariant and is spatially homogeneous and isotropic. The nonlinear polarization coupling the fields A_3 and A_4 is given by

$$P_{NL}^{(\omega_3=\omega-\delta)} = \frac{1}{2} \chi_{NL}^{(3)} A_1 A_2 A_4^{*} e^{i\{[\omega+\omega-(\omega+\delta)] t-[\vec{k}_1+\vec{k}_2-\vec{k}_4] \cdot \vec{r}\}} + \text{c.c.} \tag{22}$$

Since $\vec{k}_1 + \vec{k}_2 = 0$, the field that results when the phase mismatch is minimized will propagate along a direction opposite to that of A_4, as shown in Figure 10. A similar nonlinear polarization at frequency ω_4 results (following the procedure of Yariv and Pepper[11]) in the following set of coupled mode equations:

$$\begin{aligned} \frac{dA_3}{dz} &= i\, \kappa_3^{*} A_4^{*} e^{i\Delta kz} \\ \frac{dA_4^{*}}{dz} &= i\, \kappa_4 A_3\, e^{-i\Delta kz} \ , \end{aligned} \tag{23}$$

where the complex coupling coefficient is given by

$$\kappa_\ell^{*} = \frac{2\pi\omega_\ell}{nc} \chi_{NL}^{(3)} A_1 A_2 \ , \tag{24}$$

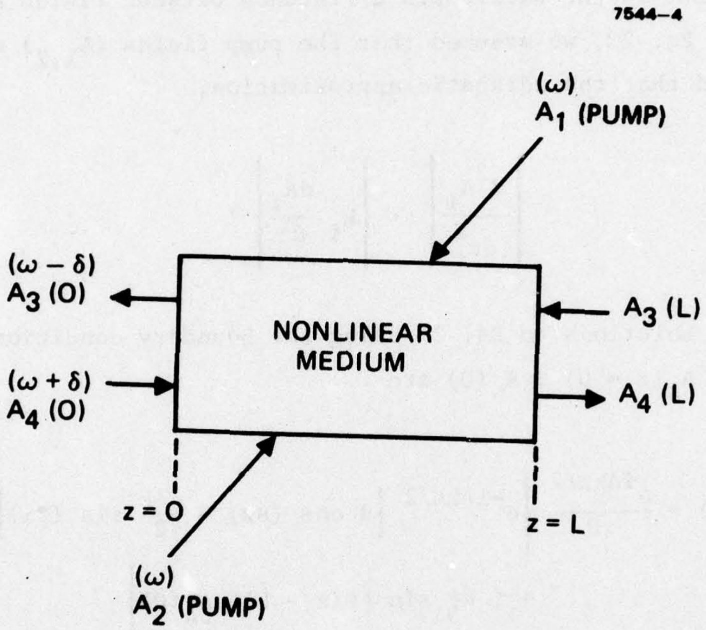

Figure 10. Nearly degenerate four-wave mixing geometry. The pump waves (at frequency ω) are assumed to be non-depleted. The probe field, A_4, is at frequency $\omega + \delta$.

and the phase mismatch is

$$|\Delta k| = 2n\pi \frac{|\Delta\lambda|}{\lambda^2} = \frac{2n\delta}{c} \ . \tag{25}$$

Note that $|\Delta\lambda|$ is the wavelength difference between fields A_3 and A_4. In arriving at Eq. 23, we assumed that the pump fields $(A_{1,2})$ are non-depleted and that the adiabatic approximation,

$$\left| \frac{d^2 A_i}{dz^2} \right| << \left| k_i \frac{dA_i}{dz} \right| ,$$

holds. The solutions to Eq. 23 using the boundary conditions of $A_3(z = L) \equiv A_3(L)$ and $A_4(z = 0) \equiv A_4(0)$ are

$$A_3(z) = \frac{e^{i\Delta kz/2}}{D} \left\{ e^{-i\Delta kL/2} \left[\beta \cos(\beta z) - \frac{i\Delta k}{2} \sin(\beta z) \right] A_3(L) \right.$$
$$\left. + \, i \, \kappa_3^* \sin[\beta(z - L)] \, A_4^*(0) \right\} \tag{26}$$

$$A_4^*(z) = \frac{e^{-i\Delta kz/2}}{D} \left\{ i\kappa_4 \, e^{-i\Delta kL/2} \sin(\beta z) \, A_3(L) + \beta\cos[\beta(z - L)] \, A_4^*(0) \right\} ,$$

where

$$D \equiv \beta \cos(\beta L) - \frac{i\Delta k}{2} \sin(\beta L)$$

and

$$\beta \equiv \sqrt{\kappa_3^* \kappa_4 + \left(\frac{\Delta k}{2}\right)^2} \ .$$

For the filter application, we assume $A_3(L) = 0$, with a single input at $z = 0$. In this case, the reflected wave at the input plane ($z = 0$) becomes

$$A_3(0) = \frac{-i\,\kappa_3^* \tan(\beta L)\, A_4^*(0)}{\beta - \frac{i\Delta k}{2}\tan(\beta L)} \quad . \tag{27}$$

We can now appreciate several filter characteristics of the four-wave interaction. First, $A_3(0)$ is proportional to $A_4^*(0)$, which implies the "near" (since $\Delta k \neq 0$) time-reversed nature of the filter output. Hence, through spatial filtering, the filter's S/N can be improved. Second, the amplitude of wave $A_3(0)$ can be greater than that of the input field (i.e., amplification) for the proper range of k_ℓ and Δk. Also, from Eq. 22, we note that the output frequency is down-shifted by the same amount as the input frequency is upshifted with respect to the pump wavelength or vice versa.

There are several useful limits that can be imposed on Eq. 26 to verify its physical nature. If, for example, we let $\Delta k \to 0$, the resultant expressions for $A_3(z)$ and $A_4^*(z)$ approach those of Yariv and Pepper,[11] where a degenerate mixing case was considered. Another useful limit is that of weak nonlinear coupling (i.e., $|\kappa_\ell/\Delta k| \to 0$. In this case, the power reflection coefficient, defined as

$$R \equiv \left|\frac{A_3(0)}{A_4(0)}\right|^2 \quad , \tag{28}$$

becomes

$$R \to |\kappa L|^2 \left(\frac{\sin\left(\frac{\Delta k L}{2}\right)}{\left(\frac{\Delta k L}{2}\right)}\right)^2 \quad . \tag{29}$$

In Eq. 29 and what follows, we set $\kappa_3 \simeq \kappa_4 \equiv \kappa$, since $\delta/\omega << 1$. We note that the $\mathrm{sinc}^2(x)$ dependence of Eq. 29 is a typical result of coherent, phase-mismatched, nondepleted interactions.[16] This result can be obtained directly by assuming in Eq. 3 that

$$\frac{dA_4^*}{dz} = 0$$

(i.e., that the perturbation of the input fields is weak) and simply integrating the remaining differential equation for $A_3(z)$. The expression in Eq. 29 is also consistent with that expected of a real-time holographic analog of the four-wave interaction.[15] The nonlinear mixing process can be viewed as forming and illuminating a real-time diffraction grating. According to Eq. 29, phase matching occurs when $(\Delta kL/2) \lesssim \pi$. Using Eq. 25, this constraint implies that the wavelength resolution of the interaction goes as $(\Delta\lambda/\lambda) \leq (\lambda/L)$. This result is consistent with the resolving power of a grating,[17] $(\Delta\lambda/\lambda) \simeq (1/mN)$, where m is the order of the grating, and N is the number of lines illuminated. The analogy can be verified by setting $m = 1$, corresponding to the first order, and realizing that $N \sim L/\lambda$ is the number of real-time "grating lines" formed in the nonlinear medium. The holographic analog only holds for $m = 1$, since higher "orders" in the nonlinear sense are phase mismatched.

The filter bandpass characteristic is obtained by using Eq. 27 in the defining expression, Eq. 28, for the power reflection coefficient, which yields

$$R = \frac{|\kappa L|^2 \tan^2(\beta L)}{|\kappa L|^2 + \left(\frac{\Delta kL}{2}\right)^2 \sec^2(\beta L)} . \tag{30}$$

Using Eq. 30, the power-reflection coefficient, R, is plotted versus a normalized wavelength detuning parameter, Ψ, for several values of the nonlinear gain, $|\kappa|L$. By definition, $\Psi = [(\Delta\lambda/2)(2nL/\lambda^2)]$, which is also equal to the phase mismatch, ΔkL, divided by 2π. The wavelength detuning parameter, $\Delta\lambda/2$, corresponds to the difference in wavelength of the probe field (A_4) relative to the pump fields ($A_{1,2}$). For an interaction length L = 1 cm, a wavelength λ = 0.5 μm, and a linear index of refraction n = 1.62 (that of CS_2), a value of unity in Figure 11 corresponds to a wavelength detuning, $\Delta\lambda/2$, of 0.0772 Å (or 9.26 GHz). The $\text{sinc}^2(x)$ form of the response holds only in the limit of weak nonlinear coupling (i.e., $|\kappa/\Delta k| << 1$). As $|\kappa|L$ increases, the bandpass becomes more sharply peaked, with the zeros of the response occurring at decreasing values of the frequency offset. This is true because the amplitude of the output wave increases with $|\kappa|L$, and the zeros of the tangent in Eq. 30 occur at smaller values of $(\Delta kL)/2$ as $|\kappa|L$ increases. The filter exhibits a power reflection coefficient exceeding unity when $|\kappa|L$ exceeds $\pi/4$ over regions of the bandpass. For CS_2 (using $\chi_{NL}^{(3)} \sim 1.8 \times 10^{-12}$ esu), $|\kappa|L = \pi/4$ corresponds to a pump intensity of ~10 MW/cm^2 (for L = 1 cm and λ = 0.5 μm). These high intensities can be realized on a cw basis by performing the filtering in an optical waveguide[18] (at a reduced FOV, limited by the numerical aperture of the waveguide). The need for high intensity can be relaxed by using resonantly enhanced, nonlinear media.

At the oscillation condition ($|\kappa|L \sim \pi/2$), a slight phase mismatch results in a drastic decrease in R, implying that oscillation has ceased. Since the phase mismatch can be the result of modifying the probe frequency and/or of varying the direction of the pump beams with respect to each other (with the concomitant change in the interaction length), beam alignment is of critical importance.[14]

The wavelength response of the filter becomes apparent if we recast the family of curves of the previous figure normalized to unity reflectivity, as shown in Figure 12. Two features are apparent. First, as $|\kappa|L$ increases, the bandwidth dramatically decreases. Second, the sidelobe structure of the filter also decreases with increasing nonlinear gain, yielding a sharper, better defined and amplified bandpass. Physically, these features occur because the filter is analogous to a real-time distributed Bragg reflecting resonator with an internal gain medium. Since the finesse of a resonator increases as gain is added to the cavity,

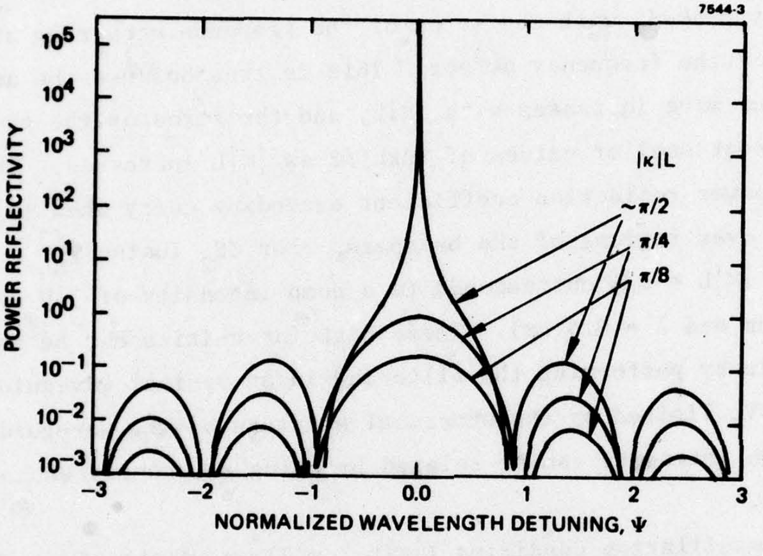

Figure 11.
Power reflectivity, R, versus normalized wavelength detuning Ψ, for several values of the nonlinear gain, $|\kappa|L$. For the example given in the text, unity along the abscissa corresponds to $\Delta\lambda/2 = 0.0772$ Å, or $\Delta\nu = 9.26$ GHz. Note that $\Psi = (\Delta\lambda/2)(2nL/\lambda^2)$.

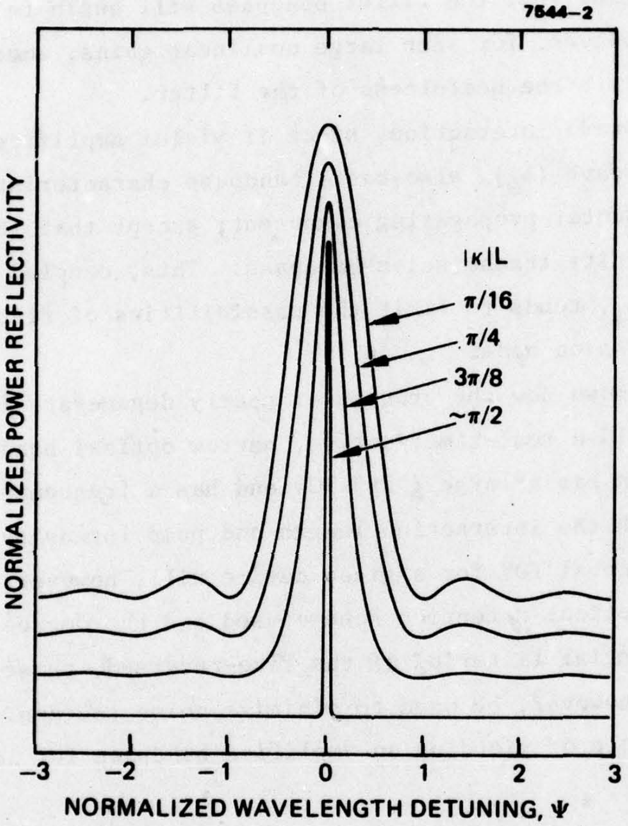

Figure 12.
Power reflectivity versus normalized wavelength detuning, Ψ, for several values of the nonlinear gain |κ|L. All curves are normalized to unity power reflectivity to emphasize the frequency bandpass of the interaction.

a sharper resonse (or Q) results.[19] As the oscillation condition is satisfied, the bandpass approaches zero, being ultimately limited by the linewidth and/or coherence length of the pump sources.

In the above discussion, we placed an upper limit of $\pi/2$ on $|\kappa|L$. When $|\kappa|L$ exceeds $\pi/2$, the filter bandpass will begin to "approximately" reproduce. However, for such large nonlinear gains, undesirable oscillation will limit the usefulness of the filter.

The four-wave interaction, since it yields amplification of the forward-going wave (A_4), also has a bandpass characteristic similar to that of its counter-propagating component, except that it is superimposed on a unity transmission bandpass. This, coupled with the lack of conjugacy of A_4, tends to limit the possibilities of filtering by means of the transmission mode.

We have shown how the process of nearly degenerate four-wave mixing can yield a real-time, active, narrow optical bandpass filter. The interaction has a large ($\sim 2\pi$) FOV and has a frequency response that depends on both the interaction length and pump intensity for a given medium. The actual FOV for a given device will, however, be limited by the specific optical detection scheme used and the degree of spatial filtering. Spatial filtering of the time-reversed, phase-conjugate output wave can, however, be used to minimize noise sources. Finally, the filter is capable of yielding an amplified bandpass for large enough nonlinear gains.

SECTION 5

CONCLUSIONS AND RECOMMENDATIONS

This section proposes a program plan for exploiting new filter concepts. We recommend an immediate demonstration program for the promising electrooptic coupled-wave filter and a lower level of effort study program for the higher risk degenerate four-wave mixing filter. The iso-index filter offers transmission and linewidth equivalent to or better than the Lyot filter, a much larger FOV, and much less complexity. In the modified coupled-wave filter, the operating wavelength is tuned away from the bandedge to eliminate absorption. This is done, however, at the expense of filter FOV. Rather than operating over 2π sr, the estimated FOV is $\sim\pm 30^{\circ}$. This is, however, the only visible filter concept that allows electronic tuning in operation. This feature may be important for accommodating unwanted wavelength shifts of the transmitter laser out of the filter passband and for controlling the effects of thermal drifts. $AgGaS_2$ is currently considered the most promising candidate material for these filters. This material has been extensively studied over the last two years at HRL on the HALO program for tunable electrooptic filters. It is presently grown in 1-in. boules, and device-quality material is available for a blue/green filter program. An important aspect of the proposed program is a comprehensive study to identify other candidate filter materials. In particular, crystals with a more rapid change in birefringence for narrower linewidth and shorter wavelength operation would be desirable.

The filter concept that offers the best potential performance is based on degenerate four-wave mixing. In principle, linewidths narrower than 0.1 Å, full 2π sr FOV, and signal amplification can be achieved simultaneously. This area, however, is the least mature and hence would be riskier than the next best alternative and would require considerable additional work. One area of great importance is the scattering of the pump lasers onto the detector by the interaction medium. Our preliminary calculation of such background noise suggests that it may be possible to obtain quantum-noise-limited performance. We recommend that this work be continued on the proposed program.

REFERENCES

1. C.H. Henry, Phys. Rev. 143, 627 (1966).
2. J.J. Hopfield and D.G. Thomas, Phys. Rev. Lett. 15, 22 (1965).
3. J.P. Laurenti, K.C. Rustagi, and M. Rouzeyre, Appl. Phys. Lett. 28, 212 (1976).
4. J.P. Laurenti, K. Rustagi, M. Rouzeyre, H. Rufer, and W. Ruppel, J. Appl. Phys. 48, 203 (1977).
5. G.D. Boyd, H. Kasper, and J.H. McFee, IEEE, J. Quantum Electron. QE-7, 563 (1971).
6. T.K. Plant, Hughes Research Laboratories, private communication.
7. S.E. Harris and R.W. Wallace, J. Opt. Soc. Am. 59, 744 (1969).
8. D.A. Pinnow, R.L. Abrams, J.F. Lotspeich, D.M. Henderson, T.K. Plant, R.R. Stephens, and C.M. Walker, Appl. Phys. Lett. 34, 391 (1979).
9. S.T.K. Nieh and S.E. Harris, J. Opt. Soc. Am. 62, 672 (1972).
10. R.W. Hellwarth, J. Opt. Soc. Am. 67, 1 (1977).
11. A. Yariv and D.M. Pepper, Opt. Lett. 1, 16 (1977).
12. R.L. Abrams and R.C. Lind, Opt. Lett. 2, 94 (1978).
13. D.M. Bloom and G.E. Bjorklund, Appl. Phys. Lett. 31, 592 (1977); S.M. Jensen and R.W. Hellwarth, Appl. Phys. Lett. 32, 166 (1978).
14. D.M. Bloom, P.F. Liao, and N.P. Economu, Opt. Lett. 2, 158 (1978); D.M. Pepper, D. Fekete, and A. Yariv, to be published in Appl. Phys. Lett.
15. A. Yariv, Opt. Commun. 25, 23 (1978).
16. A. Yariv, Quantum Electronics (Wiley, New York, 1975), pp. 421-432.
17. See, for example, F. Jenkins and H. White, Fundamentals of Optics (McGraw-Hill, New York, 1957), pp. 338-339.
18. A. Yariv, J. AuYeung, D. Fekete, and D.M. Pepper, Appl. Phys. Lett. 32, 635 (1978).
19. A. Yariv, unpublished.

APPENDIX I

DISPERSIVE REFLECTION FILTERS

A. GASES

Wavelength-selective reflection from metal vapors was first observed by R. W. Wood[A-1] nearly 70 years ago. In more recent years, this effect has been studied in detail in materials such as sodium,[A-3,A-5,A-7] cadmium,[A-2,A-6] and mercury.[A-2,A-4] In a typical experiment, the specular reflectivity at the glass/metal vapor interface is measured as a function of wavelength near a resonance line of the vapor. Due to the resonant behavior of the real and imaginary parts of the complex refractive index near the line center, the reflectivity can increase significantly from its value in the wings of the line.

A device capable of selective reflection can be thought of as a narrow-band reflection filter. Large values of skirt rejection are possible if the containing window is AR coated at normal incidence or is used at Brewster's angle. Senitzky has reported[A-8] on the properties of a filter using mercury vapor at ∿2 atm and a quartz Brewster window. The peak reflection was 14%, and the bandwidth was 0.14 Å. The skirt rejection ratio was 700 for a field of view (FOV) of 14°. However, a larger FOV would be possible if some degradation in skirt rejection ratio is acceptable. The analysis given below will make this apparent.

To calculate the variation of reflectivity with frequency, expressions relating frequency to the variation of the real and imaginary parts of the complex refractive index are required. We will restrict our consideration to the pressure-broadened regime, where the line profile is described by a simple Lorentzian line shape. Although Doppler broadening would normally need to be considered at low pressures, it need not be considered here since the refractive index variation (near resonance) is smaller at low pressures, which leads to smaller values of resonant reflectivity. If the complex refractive index is written as

$$n' = n - ik \; , \tag{A.1}$$

then the dispersion relations will be

$$n^2 - k^2 = 1 - \frac{Mx}{1 + x^2} \tag{A.2}$$

$$2nk = \frac{M}{1 + x^2} \; , \tag{A.3}$$

where

$$M = \frac{e^2 fN}{2\pi\nu_o m\gamma/2} \tag{A.4}$$

$$x = \frac{\nu - \nu_o}{\gamma/2} \; . \tag{A.5}$$

In the above expressions, x is the frequency detuning measured in terms of the linewidth γ, f is the absorption oscillator strength, N is the number density, and ν_o is the center frequency. In the collision-broadened region, the linewidth γ is proportional to the density N, and thus the factor M is a constant. This is in keeping with the well-known observation that a collision-broadened absorption line has a peak value that is independent of pressure and a linewidth that is proportional to pressure.

In the case of resonance lines, the most common type of pressure broadening is dipole-dipole (resonance) broadening. In this case, the linewidth may be written as

$$\gamma = \left(3 \frac{g_1}{g_2}\right)^{1/2} \frac{e^2 f}{2\pi\nu_o m} N \; , \tag{A.6}$$

where the g factors are the level degeneracies. Substituting into Eq. A.4 yields

$$M = \left(\frac{4}{3}\frac{g_2}{g_1}\right)^{1/2} . \tag{A.7}$$

The maximum ratio g_2/g_1 for an allowed transition is $g_2/g_1 = 3$. Substituting this value yields M = 2. Thus, the factor M is a constant and is independent of all material parameters except the level degeneracies. In this case, Eqs. A.2 and A.3 simplify to

$$n^2 - k^2 = \frac{(1 - x)^2}{1 + x^2} \tag{A.8}$$

$$2nk = \frac{2}{1 + x^2} . \tag{A.9}$$

Eqs. A.8 and A.9 have been solved for n and k as a function of x, and the results are plotted in Figure A-1. These curves are for all cases where resonance broadening applies and where $g_2/g_1 = 3$. Other types of broadening and other values of degeneracy are likely to lead to somewhat smaller variations in n and k.

At normal incidence, the reflectivity at the dielectric/metal vapor interface (with the beam entering through the dielectric) is

$$R = \frac{(n - n_1)^2 + k^2}{(n + n_1)^2 + k^2} , \tag{A.10}$$

where n_1 is the refractive index of the incident dielectric medium. This equation may, of course, be generalized to include all incident angles. In this case, there are separate relations for the reflectivity with the polarization vector in the plane of incidence (R_p) and the

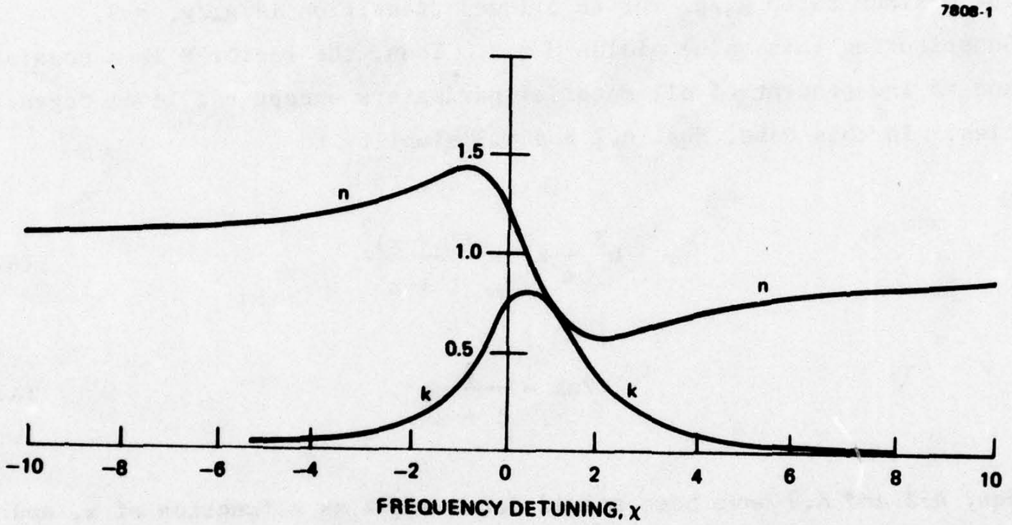

Figure A-1. Refractive index and absorption index versus normalized frequency detuning.

reflectivity with the polarization vector normal to the plane of incidence (R_s).

In Figure A-2, the reflectivity at normal incidence is plotted for waves incident in a medium with refractive index equal to 1.0 and 1.5. The former case is meant to simulate an AR-coated window, and the latter, an uncoated quartz window. The limiting values of reflectivity are near 20%, with bandwidths on the order of the collision-broadened linewidth γ. Thus, the narrowest filter bandwidth occurs at the lowest pressure where collision broadening is still dominant. This crossover point depends on the experimental conditions and on the particular gas used; the corresponding values of the linewidth are in the range from 0.05 to 0.5 Å.

We have generalized the results of Figure A-2 to include several angles of incidence. These results are shown in Figures A-3 and A-4. All angles given are measured in the incident medium. For $n_1 = 1.5$, the internal Brewster angle is 33.7°, and the critical angle is 41.8°.

Figures A-3 and A-4 suggest several observations regarding filter applications. For $n_1 = 1$ and incident angles different from zero, the reflectivity curves shift and broaden, and the peak reflectivity increases somewhat. However, the combined effects of shift and broadening are not severe for incident angles as large as 45°. For the case where $n_1 = 1.5$, the center of the FOV would be fixed at Brewster's angle ($\theta = 33.7°$), and a polarizer in the input beam would be required. Under these conditions, some shifting and broadening is again present for other angles of incidence. However, these effects are small as normal incidence is approached. We have not calculated the variation for larger incident angles (approaching the critical angle).

There are two drawbacks, apparent from Figures A-3 and A-4, to the use of selective reflection for filter applications. First, the skirt rejection rapidly degrades for incident angles differing from optimum. Second, the peak values of reflectivity are generally not higher than 10 to 30%. The skirt rejection could be improved by using a multiple-reflection configuration, but this would degrade peak reflectivity.

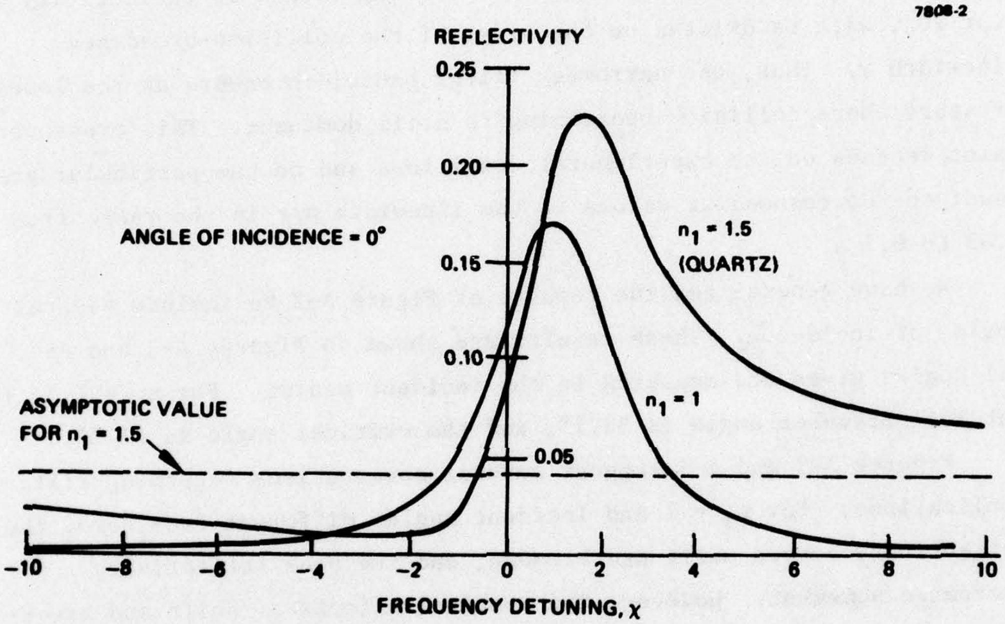

Figure A-2. Normal incidence reflectivity versus normalized frequency detuning.

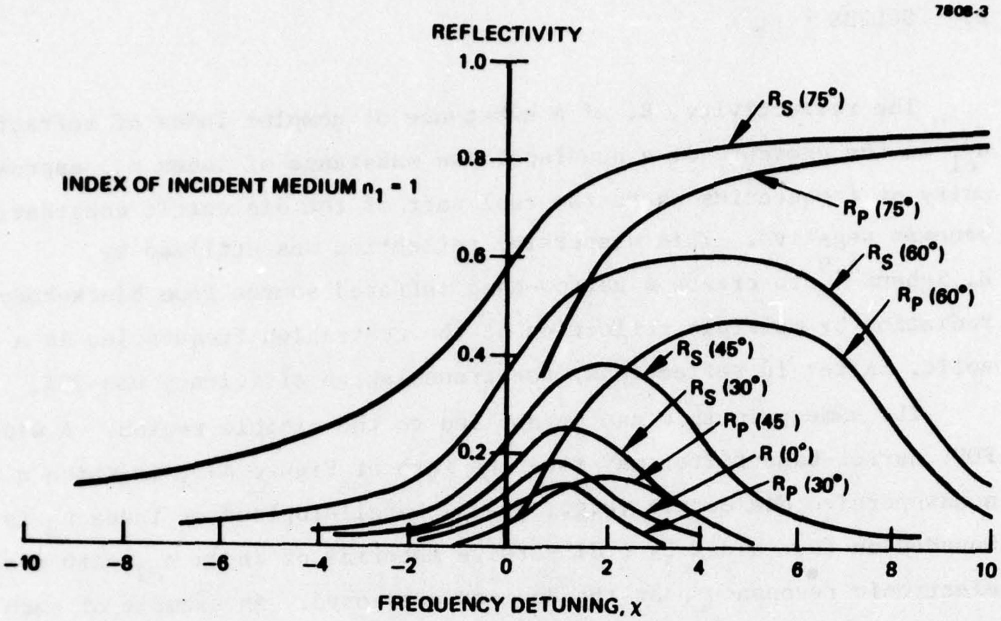

Figure A-3. Reflectivity versus frequency detuning for n_1 = 1.

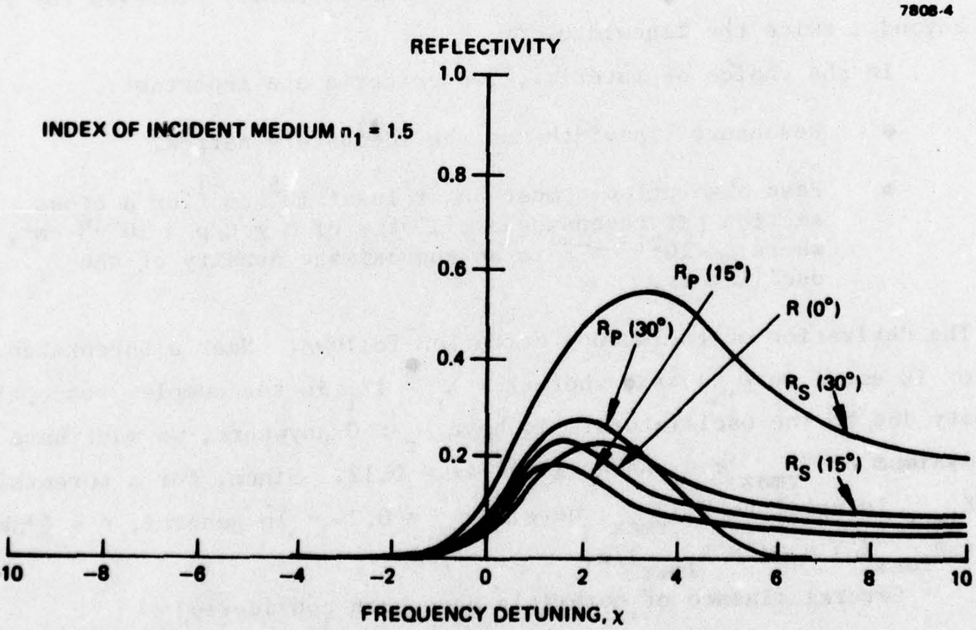

Figure A-4. Reflectivity versus frequency detuning for n_1 = 1.5.

B. SOLIDS

The reflectivity, R, of a substance of complex index of refraction n_{c1} in the presence of a nondispersive substance of index n_{c2} approaches unity at frequencies where the real part of the dielectric constant, ε_r, becomes negative. This dispersive reflection was utilized by H. Rubens[A.9] to create a narrow-band infrared source from black-body radiation by multiple reflection at the restrahlen frequencies in a solid. After 10 reflections, the transmission efficiency was 70%.

The same principle can be applied to the visible region. A wide FOV, narrow-band filter may take the form of Figure A-5, in which a nondispersive dielectric (e.g., glass) parallelopiped of index n_1 is bounded on four sides by a dispersive material of index n_{c2} with a sharp electronic resonance near the desired pass band. An example of such a resonance is shown in Figure A-6. The high reflectivity at $\varepsilon_r < 0$ is angle insensitive. The index n_1 can be chosen carefully to minimize Fresnel reflection at off-band frequencies, especially at sharp angles. A reflectivity of 10^{-3} per reflection can be easily achieved for regions beyond ± twice the linewidth, $\Delta\nu$.

In the choice of material, two criteria are important:

- Resonance linewidth must be adequately narrow.
- Peak absorption η must be at least 10^5 cm^{-1} or a cross section per resonance oscillator of $\sigma = \eta/\rho \sim 10^{-16}$ cm^2, where $\rho \sim 10^{21}$ cm^{-3} is an approximate density of the oscillators.

The derivation of the second criterion follows. Near a Lorentzian line, ε is equal to $\varepsilon_\infty + 4\pi X$, where $X = X_r - iX_i$ is the complex susceptibility due to the oscillators. To have $\varepsilon_r \leq 0$ anywhere, we must have the maximum of $X_{rmax} \geq \varepsilon_\infty/4\pi \sim (1.5)^2/4\pi = 0.12$. Since, for a Lorentzian, X_{imax} is equal to $2\ X_{rmax}$, here $X_{imax} = 0.24$. In general, $\eta = (2nk\omega/c) = (\omega\varepsilon_{imax}/c) = \omega(4\pi\ X_{imax})/c$.

Several classes of materials have been considered:

- Rare earth salt crystals, which have narrow linewidths $\Delta\nu \sim 1\text{-}2$ Å, generally have a cross section $\sigma < 10^{-18}$ cm^2, which is several orders of magnitude too small. Cooling or multiple passes could reduce the linewidth, but the weak interaction seems to rule out this approach.

8524-1

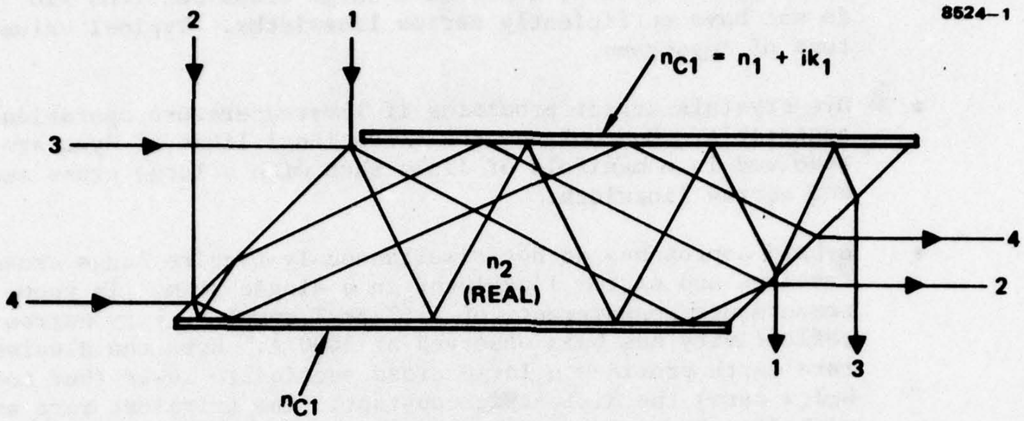

Figure A-5. Dispersive reflection filter.

8524-2

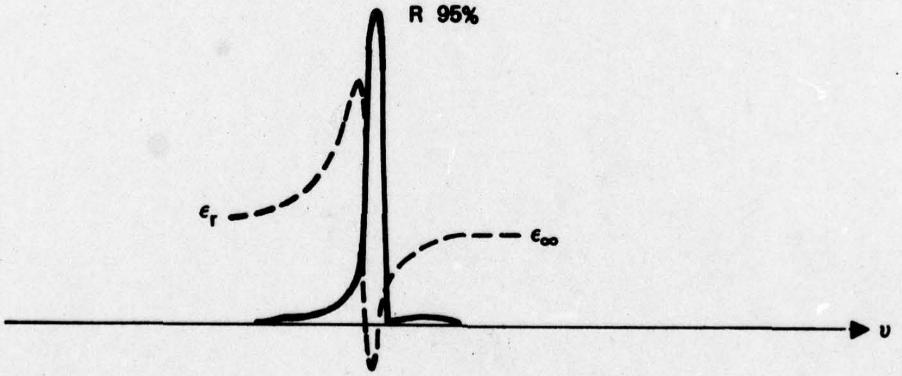

Figure A-6. Reflectivity of the dispersive reflection filter.

- Transitional metals, which have large cross sections $\sim 10^{-13}$ cm^2, do not have sufficiently narrow linewidths. Typical values are tens of Angstroms.

- Dye crystals appear promising if low-temperature operation is acceptable. On cooling, the vibrational lines of dyes are resolved in a manifold of lines each with a large cross section and narrow linewidth.

- Hybrid approaches do not simultaneously require large cross sections and narrow linewidths in a single atom. In room-temperature measurements of Er^{2+}:Er^{3+} samples, very narrow reflectivity has been observed at 3400 Å. Here the divalent rare earth provides a large cross section to lower (but not below zero) the dielectric constant. The trivalent rare earth with its narrow linewidth and modest absorption causes the reflectivity to become very high over the narrow band of interest. An attractive candidate for the blue/green portion of the spectrum is Sm^{2+}:Pr^{3+}.

The first three classes of materials present major difficulties both because their linewidths are too wide and because they require cryogenic operation. The fourth class, however, does show some, although limited, promise for future study.

APPENDIX II

INTERFEROMETER APPROACH

As noted in Appndix I, very narrow absorption lines can be obtained in solids and gases. In this approach, the problem is to take the narrow-notch absorption and transform it into a narrow passband filter. This can be done by placing the absorber in one arm of a Mach-Zehnder interferometer, as shown in Figure A-7. The interferometer must be adjusted for white-light operation — equal optical path lengths in each arm for all wavelengths of interest. Accordingly, all of the input light (the unwanted background as well as the desired signal) exits through port A and none through port B. By introducing into one arm of the interferometer an absorber that coincides with the signal wavelength, the interferometer becomes unbalanced. As a result, the signal at the desired wavelength exits through port B. However, since the interferometer is not unbalanced at wavelengths outside the narrow absorber region, all the unwanted background light continues to exit through port A. Consequently, a narrow passband filter is obtained by monitoring the signal at port B.

Both the Mach-Zehnder and the Michelson interferometers provide the second crucial element for blue-green filter applications — a relatively wide FOV. When the device is aligned for white-light operation, equal path length is maintained in the two arms for all input angles. On a ray diagram basis, FOV is limited by geometrical considerations.

Consider a plane wave with electric field E_o and radian frequency ω incident on the device, as illustrated in Figure A-7. The electric fields exiting from ports A and B are given by

$$E_A = \frac{E_o}{2} e^{i\omega t} \left[1 + e^{-\beta(\omega)L} \right] \qquad (A.11)$$

$$E_B = - \frac{E_o}{2} e^{i\omega t} \left[1 - e^{-\beta(\omega)L} \right] , \qquad (A.12)$$

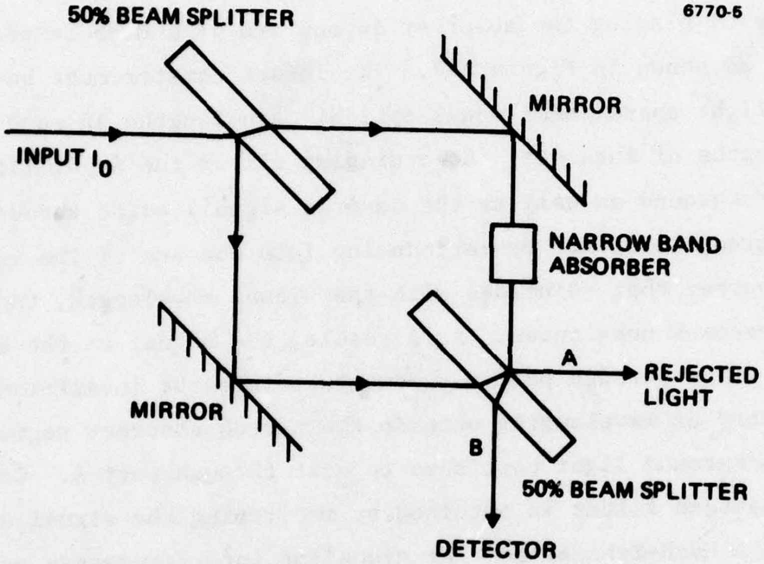

Figure A-7. The Mach-Zehnder interferometer filter.

where $\beta(\omega)$ is the complex propagation constant, and L is the length of the absorption cell. The output intensities are given by

$$I_A = \frac{1}{4} I_o \left|1 + e^{-\beta(\omega)L}\right|^2 \tag{A.13}$$

$$I_B = \frac{1}{4} I_o \left|1 - e^{-\beta(\omega)L}\right|^2 \quad . \tag{A.14}$$

The useful output of the filter clearly exits from port B and is zero if there is no absorption ($\beta = 0$).

For pure absorption (β real), the maximum output at port B will be 25%. If, on the other hand, β is pure imaginary, I_B will reach a value of 100% for $\beta L = i\pi$. For a typical spectral line, $\beta(\omega)$ is complex, and useful operation may occur in the wings of the line where the phase shift is appreciable and absorption moderate (see Figure A-8). If the Lorentzian line shape

$$\beta(x) = \beta_o \left[\frac{1}{1 + x^2} + i \frac{x}{1 + x^2}\right] \tag{A.15}$$

is assumed, where β_o is the peak field attenuation coefficient, and x is the detuning parameter normalized to the linewidth (see Eq. A.5), then the useful filter output is given by

$$\frac{I_B}{I_o} = \frac{1}{4}\left[1 - e^{\left(\frac{-2\beta_o L}{1 + x^2}\right)} - 2e^{\left(\frac{-\beta_o L}{1 + x^2}\right)} \cos\left(\frac{\beta_o Lx}{1 + x^2}\right)\right] \quad . \tag{A.16}$$

Plotting this function allows evaluating the potential maximum filter transmission and the required characteristics of the narrow-band absorber. The result is given in Figure A-9, where filter transmission is shown versus normalized detuning x for various values of $\beta_o L$, the peak absorption at line center. These curves are symmetric for ±x.

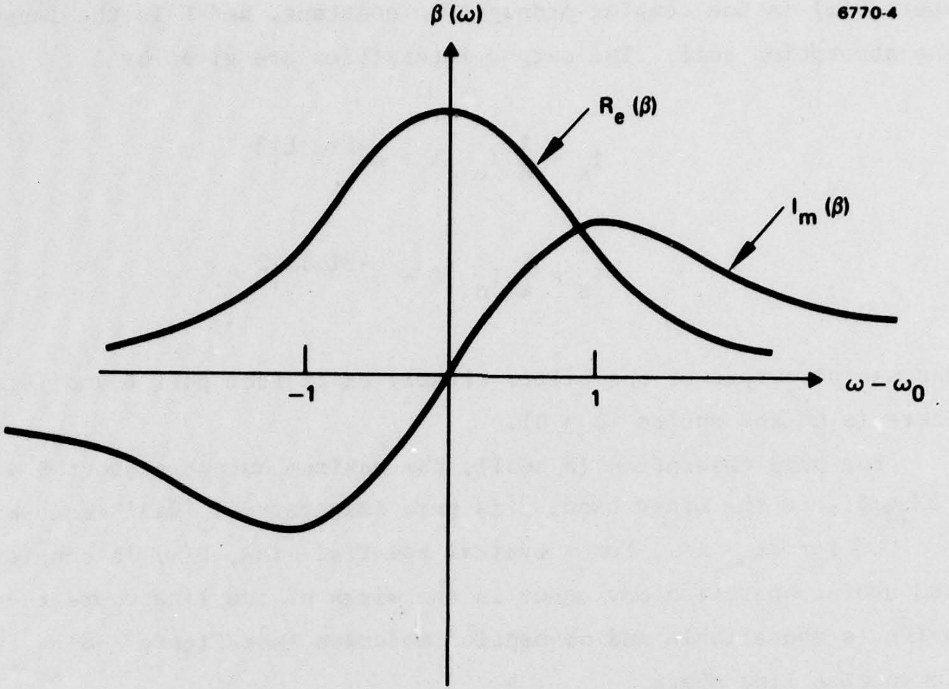

Figure A-8. Typical spectral line.

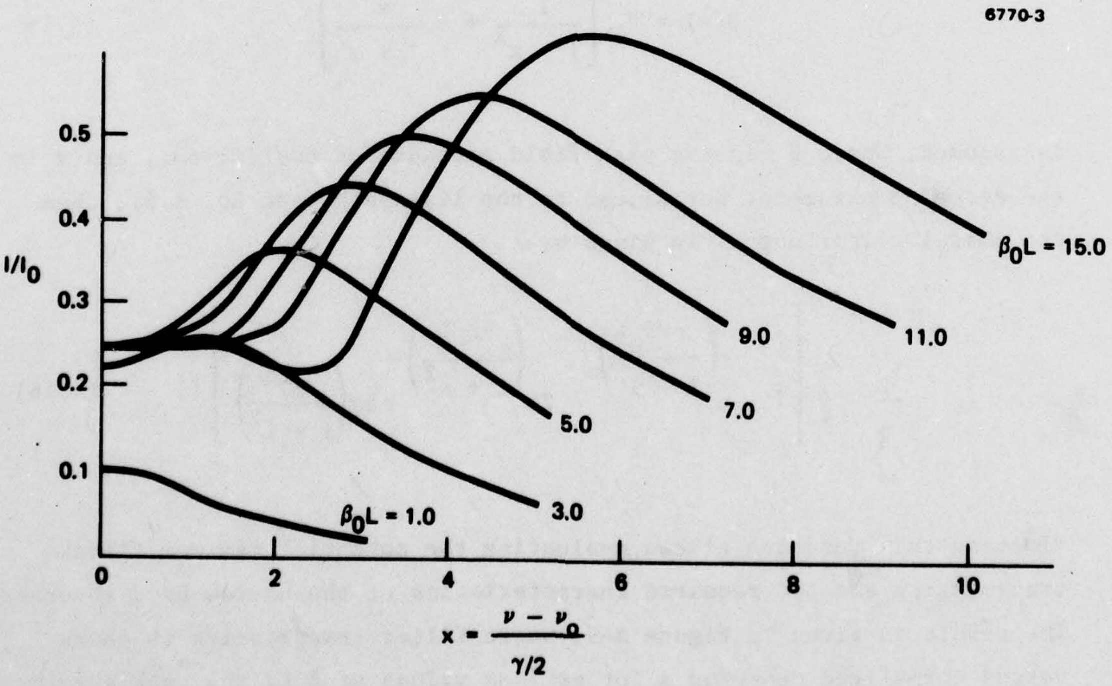

Figure A-9. Transmission versus detuning parameter.

For $\beta_o L = 1.0$, the peak transmission is 10%, decreasing monotonically to zero with approximately a Lorentzian shape. Transmission is higher, 22%, for $\beta_o L = 3.0$ at line center and increases to 26% at a detuning of $x = 1.2$. This is due to the effect of the imaginary part of β, resulting in a phase shift greater than $\pi/2$, where the cosine term in the above expression changes sign. For a very large $\beta_o L$ of 15.0, the peak phase shift exceeds 3π, so additional structure begins to appear on the transmission curves and a peak transmission of greater than 61% is obtained. Such high values of $\beta_o L$ result in optically thick samples at line center, which effectively pins the transmission to 25% over the optically thick region — which is exactly what would be expected if one beam of the interferometer were blocked.

Qualitative examination of the transmission curves reveals that a reasonable value to choose for an operating parameter is $\beta_o L = 9.0$, which would yield a peak transmission of 50% and a linewidth of $x \simeq 8$. If a bandwidth of 1 Å is desired, for example, an atomic linewidth of ~1/8 Å would be required to compensate for the increased effective linewidth of the filter operating at $\beta_o L = 9$. This value of $\beta_o L$ would require a power attenuation constant $\alpha_o L = 18$. Since sample sizes of up to 3 cm are reasonable, α_o should be greater than 6 cm^{-1}.

The ideal absorber for use in the interferometer filter would be a passive, homogeneous medium with the required narrow linewidth and high optical density contained in a single absorption feature. If use with several different sources is anticipated, then tunability would also be desirable, which would require the use of an active device. However, the advantages of an interferometer filter would be lost since the technology required to design and construct a tunable absorber could be more directly applied to construct a tunable transmission device.

Assuming that the type of laser signal source is known in advance, the most logical choice of absorbing medium for the interferometer filter would be the same medium used to produce oscillation in the laser source. There would be an automatic overlap between the source and absorber frequencies. With the possible exception of excimers, any species that can be excited to produce laser gain can also be excited to produce loss at the laser wavelength. In fact, the production of absorption is generally easier than the achievement of sufficient gain for laser action. As an example, we consider the case of a transmitter source derived from an He-N_2 charge-transfer laser oscillating on the 4709 Å line of the B-X band in N_2^+. To obtain a peak absorption of $\beta_o L = 10$ in a 10-cm length, the required population difference is $(N_{lower} - N_{upper}) \sim 4 \times 10^{13} cm^3$. It is expected that absorption at the laser frequency could be produced in an He-N_2 discharge by increasing the N_2 fraction so that charge transfer to the upper laser level is no longer dominant. The required population density should be easily obtainable at total pressures exceeding 1 atm.

Another example of a signal source in the 4700 to 4800 Å region is the argon ion laser. In particular, a strong laser transition exists at 4765 Å. For the same conditions of peak absorption and active length assumed earlier, the required absorbing population density for this transition is $2 \times 10^{11}/cm^3$. This population density can be obtained in an argon discharge run at higher pressures than optimum for laser oscillation. Similar calculations for other gases with absorption lines in the 4700 to 4800 Å region indicate that densities in the range 10^{11} to $10^{13}/cm^3$ are required. Typical linewidths for these absorption lines are in the range 0.01 to 0.05 Å, which easily meets the linewidth requirements mentioned above.

To demonstrate the relatively large ray-optics FOV possible for an interferometer, two different designs are discussed and their equivalent entrance lens speeds are computed. First, the Mach-Zehnder has an analog design that simplifies the ray-tracing geometry (see Figure A-10). The analog design would offer the advantages of simplicity and ruggedness if the narrow-band absorber could be deposited as a layer in front of the arm A mirror or contained throughout the volume of side A. If the angle at which a ray is incident on the input face is too large, then the ray will not properly pass through the interferometer. It will be necessary to provide a shield to eliminate light beyond a certain critical acceptance angle to assure proper operation. This critical angle defines the

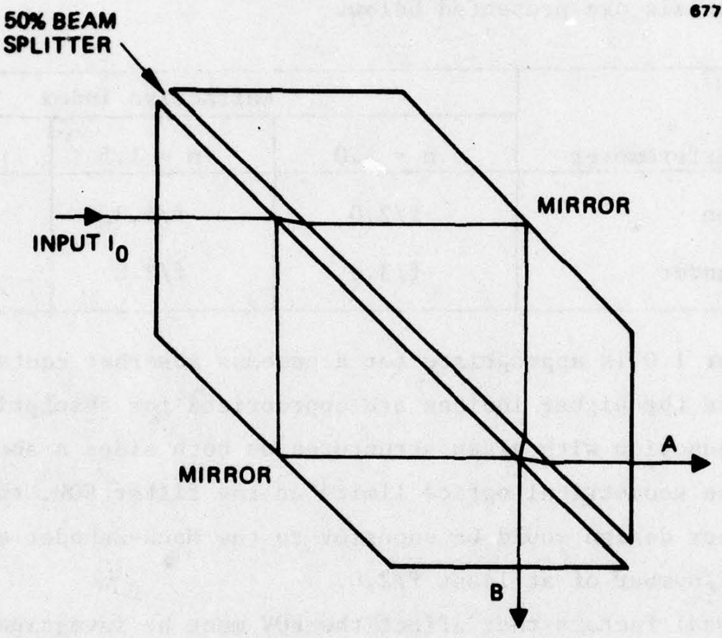

Figure A-10. A compact Mach-Zehnder interferometer.

FOV. A second design illustrating a large ray-optic FOV is that of the Michelson interferometer. Both the standard and compact designs are shown in Figure A-11. Assuming that the compact designs are constructed from material of refractive index n, the equivalent lens speed as determined by the critical ray angle of incidence has been computed. Comparative results for the Michelson and Mach-Zehnder devices using n = 1.0, 1.5, and 2.0 materials are presented below.

Interferometer	Refractive Index		
	n = 1.0	n = 1.5	n = 2.0
Michelson	f/2.0	f/1.3	f/1.0
Mach-Zehnder	f/3.0	f/2.0	f/1.5

An index near 1.0 is appropriate for a gaseous absorber contained in side A, while the higher indices are appropriate for absorption layers used in conjunction with glass structures on both sides A and B. With regard to the geometrical optics limits on the filter FOV, the Michelson interferometer design would be superior to the Mach-Zehnder and would provide an f/number of at least f/2.0.

Additional factors that affect the FOV must be investigated. The finite thickness of the beam splitter can cause the optical paths to be offset, as shown in Figure A-12. In addition, the finite thickness causes multiple reflections. If and only if this thickness is a small fraction of a wavelength will these effects be unimportant.

The interferometer approach has some distinct advantages and offers a relatively wide FOV. The need to maintain the device tuned accurately for white light fringes and to produce absorbing materials with sufficiently narrow linewidth and high absorption strength for filters considerably less than 1 Å wide are two major drawbacks to this technique. Another major drawback is that the passband for reactively dominated operation is double peaked.

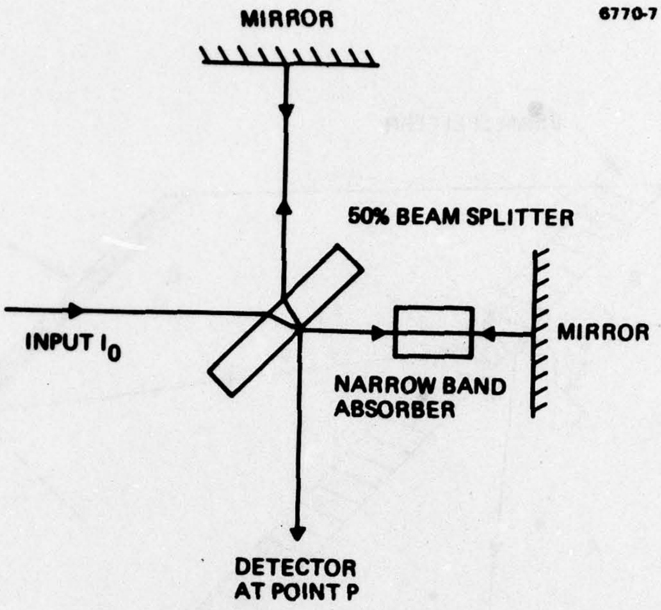

(a) STANDARD INTERFEROMETER

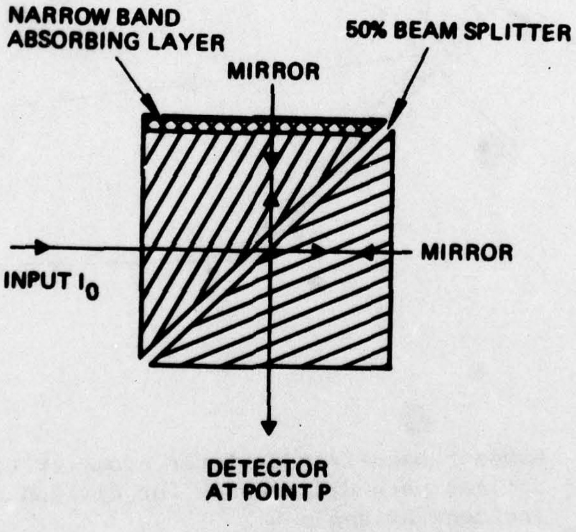

(b) COMPACT INTERFEROMETER

The A-11. The Michelson interferometer.

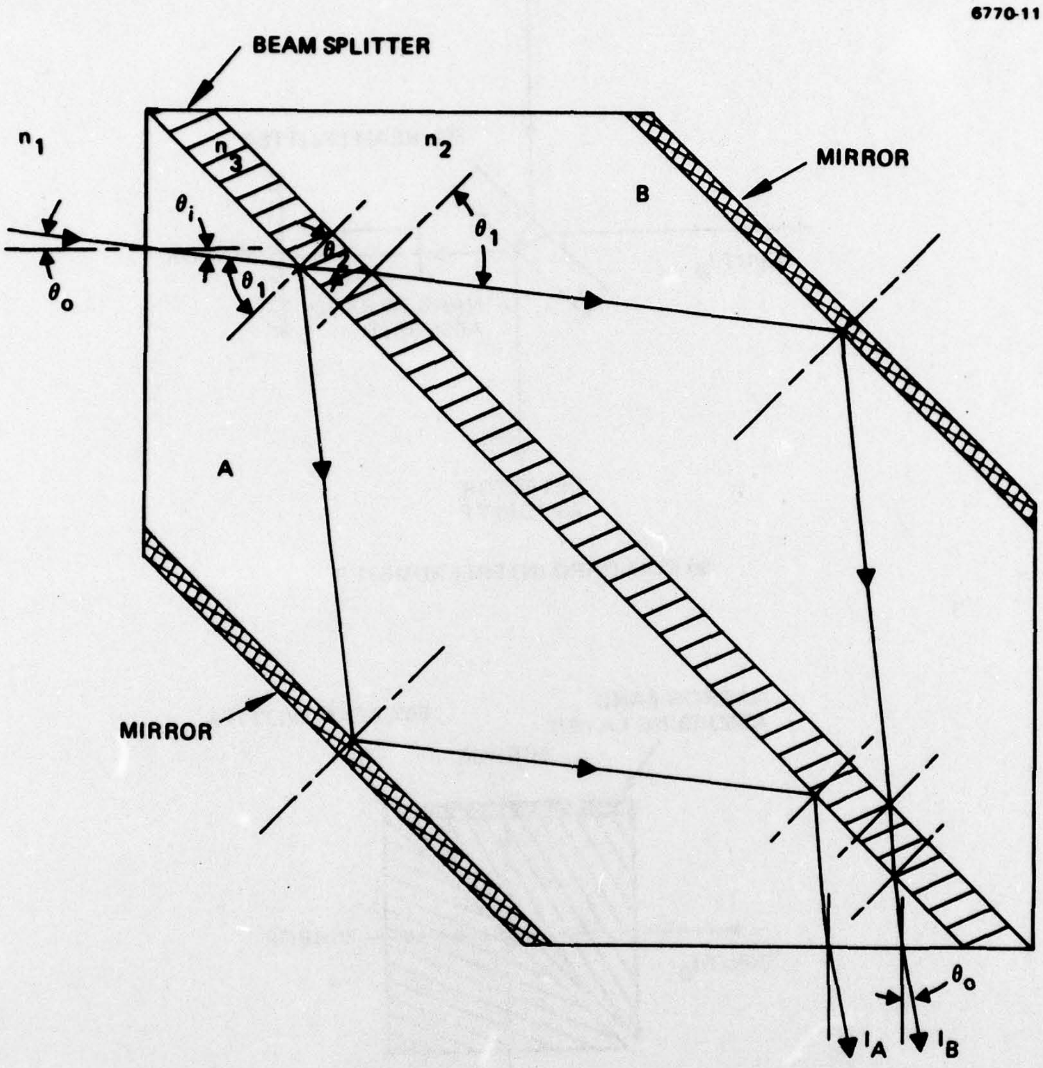

Figure A-12. Compact Mach-Zelnder interferometer filter illustrationg optical path differences for divided amplitude wave incident at angle θ_o.

APPENDIX III

HETERODYNE DETECTION

This analysis summary is intended to assess the feasibility of employing a heterodyne detection scheme as a very narrow band optical filter that also, incidentally, provides front-end gain. The field of view is, however, extremely narrow, being confined to a single resolution element of the receiver detector. In assessing various power levels, we are thus concerned exclusively with power per optical mode. We assume an i.f. bandwidth B of 10 MHz, sufficient to accommodate transmitter pulses of ~100 nsec under clear-sky conditions.

1. Noise equivalent power, NEP

$$\mathrm{NEP} = \frac{h\nu B}{\eta} \qquad \text{(A.17)}$$

$h\nu$ = photon energy = 4.4×10^{-19} J at 0.48 μm

B = i.f. bandwidth = 10 MHz

η = detector quantum efficiency ~0.5

$$\mathrm{NEP} = 8.28 \times 10^{-12} \text{ W/mode.}$$

2. Minimum local oscillator power, P_o

$$P_o \geq \frac{2\, h\nu\, k\, T_e}{q^2\, \eta\, R_d} \qquad \text{(A.18)}$$

k = Boltzmann's constant = 1.38×10^{-23} JK^{-1}

T_e = effective detector load temperature ≈ 300 K

q = electron charge = 1.60×10^{-19} C

R_d = effective detector load ~10,000 Ω

$$P_o \geq 26.7\ \mu W \ .$$

3. Background power per mode, P_m, from direct sunlight

$$P_m = \frac{2\ h\nu\ \Delta\nu}{\exp(h\nu/kT_s) - 1} = \lambda^2 N_\lambda \Delta\lambda_f \qquad \text{(A.19)}$$

T_s = effective solar temperature ~6000 K

N_λ = solar brightness = 3.185×10^3 W/cm^2-sr-μm

$\Delta\lambda_f$ = optical filter passband = 10^{-5} μm

$$P_m = 7.34 \times 10^{-11} \text{ W/mode} \ .$$

Note that this limiting level of solar flux per mode is still more than five orders of magnitude smaller than that of the local oscillator, P_o. This shows that the shot noise due to the local oscillator is the overwhelmingly dominant source of detector noise, as is required for ideal heterodyne sensitivity.

4. Seawater transmission, τ

$$\tau = \exp(-\alpha_1 \ell_1 - \alpha_2 \ell_2) \qquad \text{(A.20)}$$

α_1 = attenuation coefficient above 70 m ~ 0.07 m^{-1}

α_2 = attenuation coefficient below 70 m ~ 0.04 m^{-1}

ℓ_1 = shallow depth limit = 70 m

$\ell_1 + \ell_2$ = depth of receiver ~200 m typically

$$\tau_{200} = e^{-10.1} = 4.11 \times 10^{-5} \ .$$

5. Signal intensity at ocean surface, I_{surf}

$$I_{surf} = \frac{P_L}{A_{surf}} = \frac{W_L}{\tau_p A_{surf}} \tag{A.21}$$

P_L = peak transmitter power = 2 MW

W_L = energy per pulse = 2J

τ_p = pulse width = 10^{-6} sec maximum

A_{surf} = illuminated surface area ≈ 1 km^2 = 10^{10} cm^2

$$I_{surf} = 2 \times 10^{-4} \text{ W/cm}^2 \quad .$$

6. Estimated signal strength per mode, P_s, at submerged receiver

Our estimates are made on two bases: (a) using an apparent brightness of the source as seen from the submerged receiver, and (b) using an assumed detector area equal to the estimated coherence area at the 200-m depth.

(a) Apparent brightness of source, N_s

$$P_s = \lambda^2 N_s \Delta\lambda_s \tag{A.22}$$

The factors $N_s\Delta\lambda_s$ for the laser must be taken together and represent the effective brightness integrated over the transmitter bandwidth $\Delta\lambda_s$.

(1) Lambertian surface scatter. This represents an extreme upper limit on signal energy diffusion.

$$\begin{aligned} N_s \Delta\lambda_s &= \frac{I_{surf}\ e^{-\alpha\ell}}{\pi} \\ &= 2.6 \times 10^{-9} \text{ W/cm}^2\text{-sr} \end{aligned} \tag{A.23}$$

$$P_s = 6.0 \times 10^{-18} \text{ W/mode } (\approx 10^{-6} \text{ NEP})$$

(2) Small-angle forward scattering

$$N_s \Delta\lambda_s = \frac{I_{surf}\, e^{-\alpha\ell}}{\pi\theta_{1/2}^2} \tag{A.24}$$

$\theta_{1/2}$ = forward scatter half angle ≈ 0.2° = 0.0035 rad

$$N_s \Delta\lambda_s = 2.13 \times 10^{-4} \text{ W/cm}^2\text{-sr}$$

$$P_s = 4.9 \times 10^{-13} \text{ W/mode } (\approx 10^{-1} \text{ NEP})$$

(b) Direct attenuated plane wave on detector

$$P_s = I_{surf}\, e^{-2\ell} A_r \tag{A.25}$$

A_r = detector area ≈ 0.01 cm^2

$$P_s = 8.2 \times 10^{-11} \text{ W/mode } (\approx 10 \text{ NEP})$$

In view of the fact that the estimated minimum signal level (NEP) is 8.28 x 10^{-12} W/mode, or greater, these calculations lead to the conclusion that the heterodyne approach would be marginal at best, even under the most ideal environmental conditions.

APPENDIX IV

THE QUANTUM AMPLIFIER

Like the heterodyne receiver, the quantum amplifier can provide a very narrow optical passband, together with front-end gain. Its field of view is fairly restricted due to the nature of its tubular construction, although it can often embrace many thousands of resolution elements. As shown below, however, a laser preamplifier for a blue-green system shows little promise of providing S/N enhancement — except under conditions of extremely high background flux — because the amplifier's spontaneous emission is the dominant noise source.

The detector power signal-to-noise ratio, with a laser preamplifier of gain G_a, can be shown to take the form[A-10]

$$\frac{S}{N} = \frac{A\,G_a^2}{a + b\,G_a^2 + c(G_a - 1)^2} \quad , \tag{A.26}$$

where

$$A = \frac{\eta\,P_s^2}{2h\nu\,B\,P_B} = \left(\frac{S}{N}\right)_{BLIP} \quad (G_a = 1) \tag{A.27}$$

$$a = 1 - \xi \tag{A.28}$$

$$b = \xi + P_s/P_B \tag{A.29}$$

$$c = \frac{2h\nu_a \Delta\nu_a}{P_m} \left\{ \frac{N_2}{N_2 - N_1(g_2/g_1)} \right\} \quad , \tag{A.30}$$

P_s is the received signal power, η is the detector quantum efficiency, B is the electrical bandwidth, P_B is the background flux, and ξ is the ratio of the amplifier bandwidth to the bandwidth $\Delta\lambda_f$ of an optical filter assumed to be part of the receiver optics. The constant A is the background-limited (BLIP) S/N when $G_a = 1$. The constant c is the gain-independent portion of the amplifier spontaneous emission power per mode divided by the background power mode, P_m. The amplifier frequency and bandwidth are indicated, respectively, by ν_a and $\Delta\nu_a$. N_1 and N_2 represent the population densities of the lower and upper energy levels of the quantum transition, and g_1 and g_2 are their respective degeneracies.

It can be shown[A-10] that, in the presence of spontaneous emission, there is a maximum S/N value at an optimum gain of

$$G_a^{opt} = \frac{a + c}{c} \quad . \tag{A.31}$$

Since typically a ~ 1, c must be less than 1 to achieve any significant S/N enhancement.

Let us assume a Doppler-broadened amplifier gain profile and take as an example an Ar ion laser with a gas temperature estimated at 800 K. Then

$$\Delta\nu_a = \frac{2}{\lambda_o} \sqrt{\frac{2k\ T\ ln 2}{M}} \quad , \tag{A.32}$$

where M is the mass of the Ar ion. For $\lambda_o = 0.48$ µm,

$$\Delta\nu_a = 2.00 \times 10^9 \text{ Hz} \quad .$$

The level of background power per mode at the submerged receiver (at 200 m) is maximum when the sun is directly overhead, for which case an upper limit can be taken as

$$P_m = \lambda_o{}^2\ N_\lambda\ \Delta\lambda_f\ e^{-\alpha\ell} \quad , \tag{A.33}$$

where N_λ is the solar brightness. From Appendix III, the following values

$$N_\lambda = 3.185 \times 10^3 \ \mathrm{W/cm^2\text{-}sr\text{-}\mu m}$$

$$\alpha \ell = 10.1$$

were given. If we assume, rather generously, a filter bandwidth $\Delta\lambda_f = 10^{-4}$ µm, then

$$P_m = 3.02 \times 10^{-14} \ \mathrm{W} \quad .$$

Since the spontaneous emission factor $N_2/[N_2 - N_1(g_2/g_1)]$ is greater than 1,

$$c > \frac{2h\nu_a \Delta\nu_a}{P_m} = 5.5 \times 10^4 >> 1 \quad .$$

Clearly, since c is much greater than 1, the optimum value of gain is

$$G_a^{opt} = 1 \quad ,$$

and there is no S/N enhancement available with this particular type of amplifier. We would need a quantum amplifier with a bandwidth $\Delta\nu_a$ six orders of magnitude smaller or a background power P_m six orders of magnitude larger to realize a signficant S/N enhancement. The first condition is inherently unrealizable; the second is not representative of any realistic scenario.

APPENDIX REFERENCES

A.1. R.W. Wood, Phil. Mag. 18, 187 (1909).

A.2. H.L. Welsh, T. Kastner and A.C. Lauriston, Can. J. Research 28A, 93 (1950).

A.3. A.C. Lauriston and H.L. Welsh, Can. J. Physics 29, 217 (1951).

A.4. J.A. Galt and H.L. Welsh, Can. J. PHysics 35, 98 (1957).

A.5. A.L.J. Burgmans and J.P. Woerdman, J. de Physique 37, 677 (1976).

A.6. W. Heering, Z. Physik B20, 69 (1975).

A.7. J.P. Woerdman and M.F.H. Schuurmans, Opt. Commun. 14, 248 (1975).

A.8. B. Senitzky, Appl. Phys. Lett. 24, 68 (1974).

A.9. See, for example, H. Rubens, Das Ultrarot Spektrum (Springer, Berlin 1930).

A.10. J.F. Lotspeich, IEEE J. Quantum Electron. QE-13, 371 (1977).

[redacted]

DISTRIBUTION LIST

Scientific Officer 1 copy
Naval Research Laboratory
Attn: Code N00014
Washington, DC 20375

Administrative Contracting Officer 1 copy
Naval Research Laboratory
Attn: Code FY1767
Washington, DC 20375

Director 6 copies
Naval Research Laboratory
Attn: Code 2627/N00173
Washington, DC 20375

Director 3 copies
Defense Advanced Research Projects Agency
Attn: Technical Library
1400 Wilson Blvd.
Arlington, VA 22209

Office of Naval Research 3 copies
Physics Program Office (Code 421)
800 North Quincy Street
Arlington, VA 22217

Office of Naval Research 1 copy
Assistant Chief for Technology (Code 200)
800 North Quincy Street
Arlington, VA 22217

Naval Research Laboratory 3 copies
Department of the Navy
Attn: Technical Library
Washington, DC 20375

Office of the Director of Defense Research and Engineering 3 copies
Information Office Library Branch
The Pentagon
Washington, DC 20301

U.S. Army Research Office 2 copies
Box 12211
Research Triangle Park
North Carolina 27709

Defense Documentation Center 12 copies
Cameron Station (TC)
Alexandria, VA 22314

Director, National Bureau of Standards 1 copy
Attn: Technical Library
Washington, DC 20234

Commanding Officer 3 copies
Office of Naval Research Branch Office
536 South Clark Street
Chicago, IL 60605

Commanding Officer 3 copies
Office of Naval Research Branch Office
1030 East Green Street
Pasadena, CA 91101

San Francisco Area Office 3 copies
Office of Naval Research
One Halldle Plaza
Suite 601
San Francisco, CA 94102

Commanding Officer 3 copies
Office of Naval Research Branch Office
666 Summer Street
Boston, MA 02210

New York Area Office 1 copy
Office of Naval Research
715 Broadway, 5th Floor
New York, NY 10003

Director 1 copy
U.S. Army Engineering Research and
Development Laboratories
Attn: Technical Documents Center
Fort Belvoir, VA 22060

ODDR&E Advisory Group on Electron Devices 3 copies
201 Varick Street
New York, NY 10014

Air Force Office of Scientific Research 1 copy
Department of the Air Force
Bolling AFB, DC 22209

Air Weapons Laboratory 1 copy
Technical Library
Kirtland Air Force Base
Albuquerque, NM 87117

Air Force Avionics Laboratory 1 copy
Air Force Systems Command
Technical Library
Wright-Patterson Air Force Base
Dayton, OH 45433

Lawrence Livermore Laboratory 1 copy
Attn: Dr. W.F. Krupke
University of California
P.O. Box 808
Livermore, CA 94550

Harry Diamond Laboratories 1 copy
Technical Library
2800 Powder Mill Road
Adelphi, MD 20783

Naval Air Development Center 1 copy
Attn: Technical Library
Johnsville
Warminster, PA 18974

Naval Weapons Center 1 copy
Technical Library (Code 753)
China Lake, CA 93555

Naval Training Equipment Center 1 copy
Technical Library
Orlando, FL 32813

Naval Underwater Systems Center 1 copy
Technical Library
New London, CT 06320

Commandant of the Marine Corps 1 copy
Scientific Advisor (Code RD-1)
Washington, DC 20380

Naval Ordnance Station 1 copy
Technical Library
Indian Head, MD 20640

Naval Postgraduate School 1 copy
Technical Library (Code 0212)
Monterey, CA 93940

Naval Missile Center 1 copy
Technical Library (Code 5632.2)
Point Mugu, CA 93010

Naval Ordnance Station Technical Library Louisville, KT 40214	1 copy
Commanding Officer Naval Ocean Research & Development Activity Technical Library NSTL Station, MS 39529	1 copy
Naval Explosive Ordnance Disposal Facility Technical Library Indian Head, MD 20640	1 copy
Naval Ocean Systems Center Technical Library San Diego, CA 92152	1 copy
Naval Surface Weapons Center Technical Library Dahlgren, VA 22448	1 copy
Naval Surface Weapons Center (White Oak) Technical Library Silver Spring, MD 20910	1 copy
Naval Ship Research and Development Center Central Library (Code L42 and L43) Bethesda, MD 20084	1 copy
Naval Avionics Facility Technical Library Indianapolis, IN 46218	1 copy